Revision 3

Oxygen-fugacity evolution of magmatic Ni-Cu sulfide deposits in East Kunlun: insights from Cr-spinel composition

Lihui Jia [a] *, Yi Chen[a, b] *, Bin Su [a], Qian Mao [a], Di Zhang [a]

[a] State Key Laboratory of Lithospheric Evolution, Institute of Geology and Geophysics, Chinese Academy of Sciences, Beijing 100029, China

[b] University of Chinese Academy of Sciences, Beijing 100049, China

* Corresponding author: Lihui Jia, Yi Chen

E-mail: jialihui@mail.iggcas.ac.cn, chenyi@mail.iggcas.ac.cn

Abstract

In this study, we use Cr-spinel as an efficient indicator to evaluate the oxygen fugacity evolution of the Xiarihamu Ni-Cu deposit and the Shitoukengde non-mineralized intrusion. Oxygen fugacity is calculated using olivine-spinel oxybarometer, with spinel $Fe^{3+}/\Sigma Fe$ ratios determined by a secondary standard calibration method using electron microprobe. Cr-spinel $Fe^{3+}/\Sigma Fe$ ratios of the Xiarihamu Ni-Cu deposit vary from 0.32±0.09 to 0.12±0.01, corresponding to magma fO_2 values ranging from ΔQFM+2.2±1.0 to ΔQFM-0.6±0.2. By contrast, those of the Shitoukengde mafic-ultramafic intrusion increase from 0.07±0.02 to 0.23±0.04, corresponding to magma fO_2 varying from ΔQFM-1.3±0.3 to ΔQFM+1.0±0.5. A positive correlation between fO_2 and Cr-spinel $Fe^{3+}/\Sigma Fe$ ratios suggests that the Cr-spinel $Fe^{3+}/\Sigma Fe$ ratios can be used as an indicator for magma fO_2. The high fO_2

(QFM+2.2) of the harzburgite in the Xiarihamu Ni-Cu deposit suggests that the most primitive magma was characterized by relatively oxidized conditions, and then became reduced duirng magmatic evolution, causing S saturation and sulfide segregation to form the Xiarihamu Ni-Cu deposit. The evolution trend of the magma fO_2 can be reasonably explained by metasomatism in mantle source by subduction-related fluid and addition of external reduced sulfur from country gneisses (1.08–1.14 wt.% S) during crustal processes. Conversely, the primitive magma of the Shitoukengde intrusion was reduced and gradually became oxidized (from QFM-1.3 to QFM+1.0) during crystallization. Fractional crystallization of large amounts of Cr-spinel can reasonably explain the increasing magma fO_2 during magmatic evolution, which would hamper sulfide precipitation in the Shitoukengde intrusion. We propose that the temporal evolution of oxygen fugacity of the mantle-derived magma can be used as one of the indicators for evaluating metallogenic potential of Ni-Cu sulfide deposits, and reduction processes from mantle source to shallow crust play an important role in the genesis of magmatic Ni-Cu sulfide deposits.

Keywords: Oxygen fugacity; Cr-spinel; Ultramafic rocks; Ni-Cu sulfide deposit; East Kunlun

1 Introduction

Sulfur (S), occurring as either sulfide (S^{2-}), sulfate (S^{6+}) in silicate melts, or sulfite (S^{4+}) in volcanic gases, is a complex but key element in magmatic systems (e.g., Carroll and Rutherford, 1988; Symonds et al., 1994; Jugo et al., 2010). The behavior of chalcophile and siderophile elements (e.g., Ni, Cu, Au, Pt, and Pd) in magma is dictated by S as sulfide, and sulfide saturation exerts a primary control on the genesis of metalliferous deposits, especially for Ni-Cu-platinum group element (PGE) deposits (Imai, et al., 1993; Sillitoe, 1997; Clemente et al., 2004; Mungall et al., 2005; Li and Ripley, 2009; Taranovic et al., 2016). Jugo (2009) declared that sulfur speciation is strongly controlled by the oxidation state of magma, often expressed in terms of oxygen fugacity (fO_2). Transition from sulfide to sulfate in silicate melts occurs over a narrow fO_2 interval, and sulfide and sulfate in magma correspond to low (≤QFM) and high oxygen fugacity (>QFM+2) conditions, respectively, where QFM is the quartz-fayalite-magnetite buffer (e.g., Carroll and Rutherford, 1987; Mavrogenes and O'Neill, 1999; Matjuschkin et al., 2016; Jugo, 2009; Sun, 2020). The sulfur solubility under the latter condition is an order of magnitude higher than that under the former one (Jugo, 2009; Jugo et al., 2010). Therefore, sulfur saturation leading to sulfide segregation is more likely to occur in reduced magma than in oxidized magma (Liu et al., 2007; Jugo, 2009; Naldrett, 2011; Brenan and Caciagli, 2000; Tomkins et al., 2012). However, several Ni-Cu deposits appear to have formed in a relatively oxidized environment (>QFM), such as the Heishan and Mirabela deposits (Xie et al., 2014; Barnes et al., 2013). In addition, from partial melting in the mantle to emplacement in the shallow crust, the redox state of the parental magma would have undergone significant changes. In this regard, the fO_2 at a certain stage of magmatic evolution cannot be used as an index of Ni-Cu mineralization (Mungall et al., 2006;

Thakurta et al., 2008; Tomkins et al., 2012). Therefore, identifying the temporal changes in magma fO_2 is crucial for understanding the Ni-Cu mineralization mechanism.

Spinel often crystallizes throughout magmatic evolution and is relatively refractory and resistant to alteration compared to other minerals (e.g., olivine and pyroxene) (Barnes and Roeder 2001; Kamenetsky et al. 2001). Spinel oxybarometry, based on phase equilibrium between olivine, orthopyroxene, and spinel, provides one window into the oxygen fugacity of upper mantle and related mantle-derived magma (Bryndzia and Wood, 1990; Ballhaus et al., 1991). Obtaining accurate spinel $Fe^{3+}/\Sigma Fe$ ratios is especially important as minor changes in the activity of magnetite in spinel can have large effects on calculating fO_2 using spinel oxybarometry (e.g., Bryndzia and Wood, 1990; Birner et al., 2016). Since the development of Mössbauer spectroscopy to estimate the Fe^{3+} proportion in silicate melts (e.g., Mysen et al., 1985; Wood and Virgo, 1989; Canil and O'Neill, 1996; Dyar et al., 2006; McCammon et al., 2009; Gaborieau et al., 2020), several studies have utilized calibration of secondary standard samples to identify different Fe species using electron microprobe (Höfer et al., 2000; Enders et al., 2000). Therefore, spinel oxybarometry can be used to systematically monitor the fO_2 variation in different magmatic stages of Ni-Cu sulfide deposits.

The Xiarihamu deposit, the first Ni-Cu deposit discovered in East Kunlun, is the second-largest Ni deposit in China and contains ~157 million metric tons (Mt) of sulfide ore (Li et al., 2015; Feng et al., 2016; Liu et al., 2018). Previous zircon U–Pb studies yielded weighted-mean $^{206}Pb/^{238}U$ ages of 424 to 408 Ma (Supplemental Table S1, Jiang et al., 2015; Li et al., 2015; Peng et al., 2016; Song et al., 2016). Approximately 200 km east to the Xiarihamu area, the Shitoukengde mafic-ultramafic intrusion (426–420 Ma, Li et al., 2018; Zhang et al., 2018; Jia et al., 2021) was emplaced contemporaneously in a similar extensional setting (Wang et al., 2014; Jia et al., 2021), but no economic ore bodies have been found. The similar spatial and tectonic association between the Xiarihamu Ni-Cu deposit and the Shitoukengde intrusion provides an ideal opportunity to study the relationship between magma fO_2 evolution and Ni-Cu mineralization in orogens.

In this study, we present mineralogy, petrology, and fO_2 calculations of the Xiarihamu Ni-Cu deposit and the Shitoukengde intrusion in the East Kunlun orogenic belt. Olivine-spinel pairs in different magmatic stages were chosen to estimate the magma fO_2, track the changes in oxygen fugacity during magmatic evolution, and reveal its influence on the metallogenic mechanism of the Ni-Cu sulfide deposit. Our results contribute to further understanding the mechanism of Ni-Cu mineralization, and provide a new window into the study of the magmatic sulfide deposits in orogenic belts.

2 Geological background

2.1 East Kunlun orogenic belt

The E–W trending Kunlun orogenic belt extends >2000 km from central China to eastern Pakistan, and is located in the northeastern part of the Qinghai-Tibet Plateau (Fig. 1a). It is subdivided into the East Kunlun orogenic belt and West Kunlun orogenic belt by the NE–SW trending Altyn Tagh fault (Jiang et al., 1992). The East Kunlun orogenic belt is separated from the Qinling orogenic belt by the Wenquan fault. The Qaidam block and Songpan-Ganzi terrane are located to the north and south, respectively (Jiang et al., 1992; Xu et al., 2007; Fig. 1b). The E-W-trending faults divide the East Kunlun orogenic belt into North Kunlun Terrane, South Kunlun Terrane, and Central East Kunlun fault zone.

The Xiarihamu magmatic Ni-Cu sulfide deposit is located in the Central East Kunlun fault zone (Fig. 1c), which is characterized by widespread Proterozoic metamorphic basement, comprising the Mesoproterozoic Jinshuikou Group, and a number of Paleozoic to Mesozoic granite plutons. The Jinshuikou Group is dominated by granitic gneiss, schist and marble, and is intruded by Neoproterozoic granites (Chen et al., 2006a; Lu et al., 2006; Meng et al., 2013a). The Proterozoic basement is overlain by Ordovician amphibolite- to granulite-facies metamorphic rocks (Wang et al., 2004; Chen et al., 2006b, 2007; Zhang et al., 2003; Li et al., 2006; Lu et al., 2009). The Ordovician strata are unconformably overlain by terrestrial volcanics of the Early Devonian Maoniushan Formation, which is overlain by Carboniferous and Permian sedimentary and volcanic strata (Lu et al., 2009). Voluminous Paleozoic granitoids were emplaced into Proterozoic metamorphic rocks in the Central East Kunlun fault zone during Silurian to Early Devonian (Mo et al., 2007; Xu et al., 2007; Cui et al., 2011; Liu et al.,2012; Song et al., 2016).

Early Paleozoic ophiolites are exposed along the Central East Kunlun zone with ages of 518–420 Ma, implying the existence of a paleo-ocean (Fig. 1b; Yang et al., 1996; Bian et al., 2004; Zhu et al., 2005; Feng et al., 2010). Previous studies suggested that the tectonic transition from oceanic subduction to continent–continent collision occurred at 438 Ma (Liu et al., 2012, 2013a; Zhang et al., 2018) and the Wenquan eclogites (~428 Ma) were formed by this collisional event (Meng et al., 2013b). After 428 Ma, extensive Silurian basalts (428–419 Ma, Zhu et al., 2006) and Early Devonian-Middle Devonian mafic dikes (412–383 Ma, Sun et al., 2004; Zhang et al., 2013; Xiong et al., 2014; Yang et al., 2014) formed in the East Kunlun area, representing post-collisional products (Liu et al., 2013b; Peng et al., 2016; Song et al., 2016; Zhang et al., 2018).

2.2 Xiarihamu Ni-Cu sulfide ore deposit

The Xiarihamu deposit contains four mafic-ultramafic intrusions, including Xiarihamu I, II, III, and IV. The magmatic sulfide ore body is hosted within the Xiarihamu I intrusion, and the metallogenic potential of the other three intrusions remains under investigation (Peng et al., 2016; Li et al., 2015; Song et al., 2016; Liu et al., 2018). All these intrusions were emplaced into the Jinshuikou Group, which mainly consists of Neoproterozoic granitic gneiss and schist, yielding zircon U-Pb ages of 924 to 915 Ma (Wang, 2014; Wang et al., 2016).

The Xiarihamu I intrusion, composed of gabbroic and ultramafic rocks, is irregularly shaped, with a length of ~1400 m, a width of ~900 m, and a depth of 300 to 600 m (Fig. 2a). The western part of the intrusion is not exposed, and the southern part is covered with Quaternary clastic sediments. Observations of both surface outcrops and drill cores have confirmed no chilled margins between the gabbroic and ultramafic portions. The orebodies are mainly found in harzburgite and olivine orthopyroxenite. Weak sulfide mineralization occurs in lherzolite and websterite. For the websterite, Li et al. (2015) and Song et al. (2016) obtained ages of 411.6 ± 2.4 Ma and 406.1 ± 2.7 Ma, respectively.

The other three small mafic-ultramafic intrusions, with lengths less than 1,000 m and widths of 80 to 500 m, are located to the south of the Xiarihamu I intrusion. All of them are E-W trending and have rock assemblages similar to those of the Xiarihamu I intrusion, consisting mainly of pyroxenite with very weak sulfide mineralization. Zircon U-Pb dating indicated that the Xiarihamu II intrusion formed at 424 ± 1 Ma (Peng et al., 2016).

2.3 Shitoukengde mafic-ultramafic intrusion

The Shitoukengde I and II mafic-ultramafic intrusions are oval shaped at approximately 2.5×1.2 km^2 and 1.2×1.0 km^2 in size, respectively (Fig. 2b). These intrusions are emplaced into the Jinshuikou Group, which consists of the Neoproterozoic granitic gneiss and schist. This study focuses on the number I mafic-ultramafic intrusion, mainly consisting of the ultramafic portion and mafic portion. From field geological observations, the ultramafic rocks are irregularly distributed as autoliths in the gabbroic rocks, suggesting that they formed earlier than the gabbroic rocks. Jia et al. (2021) obtained zircon U-Pb ages of 420.6 ± 2.2 Ma for the gabbronorite and 420.4 ± 5.9 Ma for the olivine websterite, almost coeval with the Xiarihamu Ni–Cu sulfide deposit.

3 Petrology

3.1 Xiarihamu Ni-Cu deposit

The Xiarihamu intrusion is mainly composed of harzburgite, lherzolite, olivine orthopyroxenite, websterite, and mafic rocks, predominantly norites (Figs. 3a-g). Observations from outcrops and boreholes suggest that the mafic portion is in sharp contact with the ultramafic portion, and the cumulate peridotites were emplaced within the orthopyroxenite with sharp contacts (Song et al., 2020; Chen et al., 2021).

The harzburgite typically contains subhedral to euhedral olivine (40–50 vol.%), orthopyroxene (35–40 vol.%), clinopyroxene (< 5 vol.%), with minor Cr-spinel and amphibole. Cr-spinel occurs in the matrix or as fine-grained inclusions in orthopyroxene and olivine. No crosscutting relationships exist between the harzburgite and lherzolite, and they have similar petrographic features, except that the latter contains more clinopyroxene and less orthopyroxene than the former. The harzburgite grades into olivine orthopyroxenite, with the orthopyroxene increasing to more than 60 vol.%. The orthopyroxenite is composed of 60–80 vol.% cumulus euhedral orthopyroxene, 5–10 vol.% olivine, <10 vol.% clinopyroxene, and plagioclase, with minor amphibole and Cr-spinel (Fig. 3e). Orthopyroxene occurs as granular and poikilitic crystals, or as large oikocrysts enclosing fine-grained olivine. The websterite also shows cumulate texture and contains 50–70 vol.% orthopyroxene, 20–30 vol.% clinopyroxene, and <10 vol.% olivine, Cr-spinel, plagioclase, amphibole, and phlogopite (Fig. 3f). Clinopyroxene occurs as oikocrysts containing olivine or as granular crystals, whereas plagioclase, amphibole, and phlogopite are interstitial

DOI: https://doi.org/10.2138/am-2022-8050. http://www.minsocam.org/

phases. Sulfides occur locally as fine-grained, anhedral, interstitial phase (Figs. 3a-d). Nickel minerals are mainly pentlandite, while copper minerals consist dominantly of chalcopyrite, and iron minerals are mainly pyrrhotite.

The mafic portion is dominated by medium-grained norite with limited lithological changes. The norite contains mm-sized euhedral plagioclase (~35 vol.%), orthopyroxene (30–40 vol.%), and clinopyroxene (10–15 vol.%) (Fig. 3g), with less than 5 vol.% olivine, Cr-spinel, amphibole, and phlogopite.

3.2 Shitoukengde mafic-ultramafic rocks

The lithologies in the Shitoukengde intrusion are harzburgite, lherzolite, wehrlite, olivine websterite, clinopyroxenite, and gabbroic rocks (gabbro and gabbronorite). The ultramafic rocks are distributed in the gabbroic rocks. The boundary between the peridotites and pyroxenites is not obvious, indicating that these units formed during the same stage of magmatic evolution.

The harzburgite contains 50–55 vol.% olivine, 40–50 vol.% orthopyroxene, 3–5 vol.% clinopyroxene, and 1–2 vol.% Cr-spinel (Fig. 3h). The lherzolite is composed of 45–60 vol.% olivine, 15–20 vol.% orthopyroxene, 10–15 vol.% clinopyroxene, 5–10 vol.% plagioclase and minor amounts of Cr-spinel and phlogopite (Fig. 3i). The olivine grains are commonly enclosed in poikilitic orthopyroxene, and clinopyroxene, plagioclase, and amphibole are interstitial between olivine and orthopyroxene. The olivine websterite contains 15–20 vol.% olivine, 25–35 vol.% clinopyroxene, and 15–30 vol.% orthopyroxene, with minor (<5 vol.%) plagioclase, Cr-spinel, and phlogopite (Fig. 3k). Clinopyroxenite contains ~90 vol.% clinopyroxene, 5 vol.%

olivine, < 5 vol.% orthopyroxene, and plagioclase (Fig. 3l). Notably, the Shitoukengde ultramafic rocks have higher Cr-spinel proportions (~2.32 vol.%) than that of the Xiarihamu Ni–Cu deposit (~0.05 vol.%, Supplemental Fig. S1). Sulfides occur as fine-grained inclusions in olivine and orthopyroxene (Figs. 3h-k).

The gabbronorite contains 25–35 vol.% plagioclase, 30–40 vol.% orthopyroxene, 5–15 vol.% clinopyroxene, 2–5 vol.% olivine, and less than 5 vol.% amphibole, Cr-spinel, and phlogopite. Orthopyroxene occurs as prismatic euhedral to subhedral crystals, whereas clinopyroxene occurs as larger subhedral crystals. Gabbro comprises 45–55 vol.% clinopyroxene, 25–35 vol.% plagioclase, and minor amounts of phlogopite and Fe-Ti oxides.

3.3 Country gneisses

The Xiarihamu Ni-Cu deposit is surrounded by amphibole plagiogneiss, which is composed of plagioclase (35–45 vol.%), quartz (20–25 vol.%), amphibole (10–15 vol.%), and minor biotite (Supplemental Fig. S2). Fine-grained (10–30 μm) pyrite is commonly observed in the country gneiss. The country gneisses of the Shitoukengde intrusion include amphibole gneiss and biotite plagiogneiss in the Baishahe Formation of the Jinshuikou Group. The amphibole gneiss displays a gneissic structure and mainly consists of plagioclase, quartz, amphibole, and biotite. The biotite plagiogneiss consists of quartz (35–40 vol.%), plagioclase (25–30 vol.%), biotite (10–15 vol.%), and amphibole (<10 vol.%). No sulfide crystals were found in either type of the country gneisses.

3.4 Cr-spinel characteristics

Cr-spinel crystals are widely developed as accessory minerals in the Xiarihamu and Shitoukengde mafic-ultramafic rocks, and their main characteristics are as follows: 1) the proportion of Cr-spinel in the Shitoukengde intrusion is much higher than that in the Xiarihamu ore-bearing mafic-ultramafic rocks (~2.32 vol.% and ~0.05 vol.%, respectively, Supplemental Fig. S1); 2) Cr-spinel appears in the peridotites, pyroxenites, and gabbroic rocks, suggesting that Cr-spinel crystallized at different stages during magma evolution (Fig. 3); 3) Cr-spinel crystals commonly occur in the matrix or as fine-grained inclusions in olivine, pyroxenes and plagioclase. A small amount of Cr-spinel occurs as a cumulus phase; 4) although the olivine hosting Cr-spinel inclusions has been variably serpentinized along fractures, most Cr-spinel crystals are likely to be chemically homogeneous (Fig. 3f); and 5) some Cr-spinel grains enclosed in tschermakite and serpentine have clear compositional zoning (Figs. 3n-o), showing Mg-Al-rich core and Cr-Fe^{2+}-rich rim.

4 Methods

We analyzed the major elemental compositions of olivine and Cr-spinel at the Institute of Geology and Geophysics, Chinese Academy of Sciences using a JEOL JXA8100 electron microprobe. SiO_2, TiO_2, Al_2O_3, Cr_2O_3, V_2O_3, FeO, MnO, CaO, MgO, NiO, Na_2O, and K_2O were analyzed using a voltage of 15 kV, a beam current of 20 nA, a spot size of 1 μm and a 10–30 s peak counting time. The detection limits were 182 ppm for Na, 168 ppm for Si, 209 ppm for Cr, 132 ppm for K, 144 ppm for Mg, 215 ppm for Mn, 173 ppm for Ca, 152 ppm for Al, 204 ppm for Fe, 240 ppm for

Ti, and 257 ppm for Ni, respectively. The natural minerals and synthetic oxides used for calibration are as follows: diopside (Ca, Si, and Mg), albite (Na and Al), rutile (Ti), bustamite (Mn), K-feldspar (K), NiO (Ni), Fe_2O_3 (Fe), Cr_2O_3 (Cr), and V_2O_5 (V). A program based on the ZAF procedure was used for data correction (CITIZAF, Armstrong, 1995). The estimated precisions for major elements and trace elements are ±2% and ±10%, respectively.

Spinel $Fe^{3+}/\Sigma Fe$ ratios are commonly determined by the charge imbalance method with electron probe microanalysis (EPMA) data, which would lead to large uncertainties in the $Fe^{3+}/\Sigma Fe$ ratios. Wood and Virgo (1989) presented a correction procedure for increasing the accuracy of EPMA measurements involving the analysis of a spinel standard set previously characterized for $Fe^{3+}/\Sigma Fe$ ratios by Mössbauer spectroscopy. They reported a linear correlation between the difference in the $Fe^{3+}/\Sigma Fe$ ratio measured by Mössbauer and that calculated by EPMA analysis. Davis et al. (2017) systematically assessed this correction method, and suggested that it can improve the precision of the spinel $Fe^{3+}/\Sigma Fe$ ratios determined by EPMA. While creating the secondary standard calibration method, we tested the reproducibility of this method (Supplemental Table S2 and Fig. S3). A total of 8 Cr-spinel standard samples from a wide range of geographic and tectonic environments (MBR8307, HR04-08, SC1-27, BAR8601-9, MHP79-4, IM8703, VI314-58, and MO4500-24) with known $Fe^{3+}/\Sigma Fe$ ratios were tested (Wood and Virgo, 1989), and each sample was tested at 10 points by EPMA (Supplemental Table S3). Meanwhile, the spinel $Fe^{3+}/\Sigma Fe$ ratios were calculated based on the perfect stoichiometry. The average ratios

DOI: https://doi.org/10.2138/am-2022-8050. http://www.minsocam.org/

of spinel standard samples were compared with those obtained by Mössbauer spectrometry, and a linear correction relationship was established. After correction, the spinel $Fe^{3+}/\Sigma Fe$ ratios by EPMA were nearly identical to those by Mössbauer spectroscopy (Fig. 4). The precision of the $Fe^{3+}/\Sigma Fe$ ratios averages within 0.04 (2σ). Then, this equation was used to accurately correct the $Fe^{3+}/\Sigma Fe$ of the unknown Cr-spinel samples.

Whole-rock S concentrations were determined by high frequency combustion-infrared absorption using an HIR-944B carbon-sulfur analyzer at the National Research Center of Geoanalysis in Beijing, China. The analytical uncertainty was within ±10% of the accepted values, based on the results from the national standard (GBW07306) analyzed together with our samples. The detection range varies from 0.0013 to 2.0 wt.%.

5 Results

Olivine from different rock units in the Xiarihamu deposit forms a fractional crystallization trend, showing that forsterite (Fo) values decrease from 89.8±0.4–86.6±0.0 in harzburgite to 87.6±0.3–87.2±0.1 in olivine orthopyroxenite, 87.4±0.5–86.7±0.1 in lherzolite, 85.2±0.5–83.6±0.1 in websterite and 83.9±0.1–83.3±0.0 in norite, respectively (Supplemental Table S4). Olivine contains 43.5–48.8 wt.% MgO, 9.72–15.9 wt.% FeO, 0.13–0.36 wt.% NiO, and 0.13–0.22 wt.% MnO. The average olivine Fo values of the Shitoukengde intrusion decrease systematically from 88.9±0.1 in harzburgite to 85.2±0.3 in lherzolite, 84.5±0.4 in olivine websterite, 81.8±0.3 in clinopyroxenite and 77.6±0.3 in gabbronorite. The olivines have MgO

DOI: https://doi.org/10.2138/am-2022-8050. http://www.minsocam.org/

contents of 38.9±0.5 to 48.5±0.4 wt.%, FeO contents of 10.5±0.0 to 22.0±4.3 wt.% NiO contents of 0.14±0.03 to 0.27±0.04 wt.%, and MnO contents of 0.15±0.00 to 0.30±0.07 wt.%.

Cr-spinel grains are rare in the Xiarihamu mafic-ultramafic rocks. The Cr-spinels from both the harzburgite and olivine orthopyroxenite have similar Cr# [molar, 100× Cr/(Cr+Al)] (42.8±1.5–52.5±5.4 and 41.3±3.1–45.6±5.6, respectively), which are higher than those in the lherzolite (38.5±2.3–39.6±12.5), websterite (11.1±0.6–30.7±7.4) and norite (17.5±0.1–22.1±10.2), decreasing with the decrease of Fo value in coexisting olivine. The decrease of spinel Cr# values in these rocks is coupled with decreasing FeO (16.6–33.3 wt.%), Cr_2O_3 (7.18–42.2 wt.%), and increasing Al_2O_3 (22.1–57.1 wt.%) and MgO (7.53–16.0 wt.%). The $Fe^{3+}/\Sigma Fe$ ratios in Cr-spinel vary from 0.12±0.01 to 0.32±0.09, showing a positive correlation with spinel Cr#. The studied Cr-spinel grains appear homogenous under backscattered electron images, but the cores exhibit overall higher $Fe^{3+}/\Sigma Fe$ ratios than those of rims in some Cr-spinel grains (Figs. 5a-b). In addition, the $Fe^{3+}/\Sigma Fe$ ratios also decrease from the core to rim in the individual Cr-spinel grains (Figs. 5c-d).

Cr-spinel grains are common in the Shitoukengde intrusion and contain 34.1±0.4–42.0±5.2 wt.% Al_2O_3, 17.5±0.6–33.4±12.2 wt.% Cr_2O_3, and 8.13±0.32–14.9±3.6 wt.% MgO, with Cr# varying between 22.7±1.2 and 39.6±15.2 (Supplemental Table S5). The FeO concentrations vary between 16.2±0.5 wt.% and 30.4±1.9 wt.%, and display a negative correlation with the coexisting olivine Fo value, which is different from the positive correction between Cr-spinel FeO and olivine Fo in the Xiarihamu intrusion.

The $Fe^{3+}/\Sigma Fe$ ratios in Cr-spinel vary from 0.07±0.02 to 0.23±0.04, increasing as the olivine Fo values decrease. No systematic variation is observed with $Fe^{3+}/\Sigma Fe$ ratios of core-to-rim in the individual Cr-spinel grain.

The country rocks of the Xiarihamu Ni-Cu deposit are Neoproterozoic granitic gneisses and have high whole-rock S contents (1.08–1.14 wt.%). In contrast, the whole-rock S contents of the country rocks of the Shitoukengde intrusion are relatively low, varying from 0.005 to 0.018 wt.% (Supplemental Table S6).

6 Discussion

6.1 Calculation of the oxygen fugacity

Before using olivine-spinel oxybarometry to calculate the magma fO_2, it is necessary to estimate the temperature and pressure of the corresponding magma. We calculated the temperature for each sample using the olivine-spinel thermometer of Li et al. (1995). The calculated temperatures of the Xiarihamu and Shitoukengde mafic-ultramafic intrusions vary from 1016 to 869°C and 1038 to 702°C, respectively, which represent the equilibrium temperatures between olivine and Cr-spinel. A positive correlation is observed between the calculated temperatures and olivine Fo values (Supplemental Fig. S4). As mafic-ultramafic cumulate rocks lack a good barometer, we assumed a pressure of 100 MPa for all calculations following previous estimates for the Xiarihamu and Shitoukengde mafic-ultramafic intrusions (Li et al., 2015; Liu et al., 2018). The pressure effects on the calculated temperature and oxygen fugacity are approximately 2°C and 0.03 log units per 100MPa, respectively.

A difficulty sometimes encountered when calculating fO_2 is lacking an appropriate phase assemblage required for oxybarometry. Critically, Ballhaus et al. (1991) simplified the equation used to calculate fO_2 by assuming that the effect of ferrosilite activity in orthopyroxene was canceled by the effect of fayalite activity in olivine for samples with high Mg#. In this case, the oxybarometer can give reasonable results for orthopyroxene-undersaturated ultramafic rocks because the corrections rarely exceed a shift in fO_2 of -0.2 log units (Bucholz and Kelemen, 2019). Except for gabbro, all the studied samples contain olivine, orthopyroxene, and Cr-spinel, and thus are suitable for the olivine-spinel oxybarometer (Ballbaus et al., 1991; Davis et al., 2017). For gabbroic rocks, we ignore the effect of ferrosilite activity in orthopyroxene. In order to verify the accuracy of Ballhaus' equation, the fO_2 values of sulfide-mineralized ultramafic rocks from Xiarihamu Ni-Cu deposit calculated by the other Ol-Opx-Spl oxybarometer from Wood (1990) are consistent with our results, as shown in Fig. 6a and Supplemental Table S7.

Of particular concern for this study is the potential that subsolidus cooling may drive a change in fO_2 and variations in mineral chemistry in magmatic rocks (Roeder and Campbell, 1985; Lindsley and Frost, 1992; Birner et al., 2018; Hou et al., 2021). Subsolidus equilibration between olivine and spinel was first considered by Irvine (1965), who described Mg^{2+} diffusion from spinel to olivine and Fe^{2+} diffusion from olivine to spinel. Bucholz and Kelemen (2019) found that subsolidus exchange reactions increased calculated fO_2 by 0.3–0.35 log units over 300℃ of cooling. However, assuming constant modal percentages of minerals, subsolidus cooling would decrease the Fe^{2+} content of olivine and increase Fe^{2+} content of spinel, which is not observed in the Shitoukengde and Xiarihamu ultramafic intrusions (Supplemental Figs. S5a-b). In addition, the compositional profiles from core to rim of the Cr-spinel grains in the Xiarihamu intrusion reveal decrease in FeO (Supplemental Figs. S5c-d). These lines of evidence argue against the trend of the Mg-Fe exchange between olivine and spinel. Furthermore, almost 80% EPMA analysis spots of the spinel and olivine grains were analyzed in the cores, which represent the most primitive compositional information. Therefore, we believe that subsolidus exchange of Fe-Mg between olivine-spinel pairs has negligible influence on the calculated fO_2 of the Shitoukengde mafic-ultramafic intrusion and Xiarihamu Ni-Cu deposit.

Several Cr-spinel grains with clear chemical zoning (Figs. 3n-o) were not used for calculations, as they might be modified by late-stage interstitial melts (e.g., Henderson and Wood, 1981; Candia and Gaspar, 1997; Ahmed et al. 2008; Mukherjee et al., 2010). Cr-spinel grains showing no visible zoning under BSE imaging were chosen to calculate the magma fO_2 (Figs. 3a-j). The Cr-spinel $Fe^{3+}/\Sigma Fe$ ratios of the Xiarihamu Ni-Cu deposit vary from 0.32±0.09 to 0.12±0.01, corresponding to magma fO_2 values from ΔQFM+2.2±1.0 to ΔQFM-0.6±0.2. By contrast, those of the Shitoukengde mafic-ultramafic intrusion increase from 0.07±0.02 to 0.23±0.04, corresponding to magma fO_2 varying from ΔQFM-1.3±0.3 to ΔQFM+1.0±0.5. Notably, the calculated magma fO_2 and Cr-spinel $Fe^{3+}/\Sigma Fe$ ratios show a positive correlation (Supplemental Fig. S6). Therefore, we suggest that the Cr-spinel $Fe^{3+}/\Sigma Fe$ ratios can be used as an indicator for magma fO_2. The large variations in fO_2 values enable us to evaluate the redox changes during magmatic fractionation and related sulfide mineralization.

6.2 Temporal evolution of the magma fO_2

When sulfur is saturated in mafic magma, immiscible droplets of sulfide melt exsolve, and the chalcophile elements partition from the silicate melt into the sulfide liquid (Goldschmidt, 1937; Naldrett, 2004; Tomkins et al., 2012; Kiseeva et al., 2017). Oxygen fugacity controls sulfur speciation and hence sulfur concentrations during both partial melting in the mantle source and sulfide segregation in the shallow crust (Jugo, 2009; Mungall et al., 2006; Thakurta et al., 2008; Tomkins et al., 2012). This variable has received little attention and may be crucial for understanding the Ni-Cu mineralization mechanism.

From the harzburgite, olivine orthopyroxenite, lherzolite, websterite to norite in the Xiarihamu Ni-Cu deposit, olivine-spinel pairs were selected to calculate the fO_2 in different magmatic stages. The oxygen fugacity characteristics are summarized as follows: 1) the relatively high fO_2 (ΔQFM>+1.00) recorded in the harzburgites, containing the most primitive olivines (Fo>88), suggests that the primitive magma of the Xiarihamu deposit was characterized by an oxidized environment. The fO_2 decreased with lowing olivine Fo values and shifted to a reduced environment (Fig. 6). 2) The Cr-spinel cores have slightly higher $Fe^{3+}/\Sigma Fe$ ratios and fO_2 than the rims (Figs. 5a-b). In addition, the $Fe^{3+}/\Sigma Fe$ ratios become lower from core to rim in the individual Cr-spinel grain (Figs. 5c-d). These phenomena suggest that the Ni-Cu bearing magma became reduced during crystallization. Compared to that of the Xiarihamu Ni-Cu deposit, the fO_2 of the Shitoukengde intrusion exhibits a significantly different trend. The calculated results show that the initial crystallization products formed in a reduced environment (Fo=88.9±0.1, ΔQFM=-0.9±0.5), with fO_2 gradually increasing during crystallization (Fig. 6).

In summary, the primitive magma of the Xiarihamu Ni-Cu deposit progressively changed from an oxidized to a reduced state, with fO_2 varying from ΔQFM+2.2±1.00 to ΔQFM-0.6±0.2, being reduced into the sulfide stability field, which would have caused sulfide segregation and ultimately ore deposit formation. Comparably, several typical Ni-Cu deposits in Central Asian Orogenic Belt also show a positive relation between magma fO_2 calculated by different oxybarometers and olivine Fo values (Fig. 6a, Xie et al., 2014; Li et al., 2015; Xue et al., 2016, 2021; Mao et al., 2017). The temporal evolution of magma fO_2 is consistent with the previous study of Tomkins et al. (2012), proposing that reduction-induced sulfide saturation can drive the formation of magmatic sulfide deposits. In contrast, the primitive magma fO_2 of the Shitoukengde intrusion was reduced and then became oxidized (from ΔQFM-1.3±0.3 to ΔQFM+1.0±0.5, Fig. 6b), which inhibited S saturation and sulfide segregation. This may be one of the most compelling reasons for the weak Ni-Cu mineralization of the Shitoukengde mafic-ultramafic intrusion.

6.3 Response of magma fO_2 to the Ni-Cu mineralization

The redox state of mantle-derived magma may be inherited from the nature of the mantle source. For instance, island arc magma always has higher magma fO_2 (ΔQFM+1–ΔFMQ+3) than mid-ocean ridge basalt (MORB, ΔQFM-2–ΔFMQ), which

This is the peer-reviewed, final accepted version for American Mineralogist, published by the Mineralogical Society of America.
The published version is subject to change. Cite as Authors (Year) Title. American Mineralogist, in press.
DOI: https://doi.org/10.2138/am-2022-8050. http://www.minsocam.org/

is generally interpreted as the mantle source of arc magma having been metasomatized by an oxidizing subduction-zone fluid (Brandon and Draper, 1996; Cottrell and Kelley, 2011; Berry et al., 2018; Evans and Tomkins, 2011; Evans, 2012; Brounce et al., 2014; Zhang et al., 2006). In addition, magma fO_2 can also be affected by later shallow processes such as crystallization differentiation (Lee et al., 2005; Jenner et al., 2010), crustal contamination (e.g., Deng et al., 2017; Tao et al., 2008; Mao et al., 2018; Zhang et al., 2009a, 2009b), and degassing (Kelley and Cottrell, 2012; Moussallam et al., 2016). Therefore, the primitive magma could have undergone a series of changes in oxygen fugacity from the mantle source to intrusion in the crust. How the evolution of magmatic oxygen fugacity controls Ni-Cu mineralization processes is poorly understood and worthy of thorough exploration. We therefore hypothesize that if the oxidized primitive magma, with high concentrations of dissolved sulfur as sulfate, could be reduced into the sulfide stability field, it would cause sulfide saturation, would lead to ore deposition.

The fO_2 values recorded by spinel-olivine pairs in the most primitive ultramafic rocks from the Shitoukengde intrusion are estimated to be ΔQFM-1.3±0.3, suggesting that the primitive magma was likely derived from a reduced mantle source. The fine-grained sulfide inclusions in olivine and orthopyroxene (Figs. 3h-i) are consistent with the reduced conditions in the magma during the early stage of crystallization. However, the fO_2 values of most primitive magma from Xiarihamu Ni-Cu deposit (ΔQFM+2.2±1.0) is much higher than that of the Shitoukengde intrusion (Fig. 6), and olivine crystals with high Fo values contain no sulfide inclusions, suggesting the primitive magma was likely derived from an oxidized mantle source. Orthopyroxenes from the Xiarihamu harzburgites have low $\delta^{26}Mg$ (–0.49 to –0.34‰, Chen et al., 2021), which is proposed to be genetically related to carbonated mantle source that probably formed by incorporation of recycled carbonates (e.g., Yang et al., 2012; Teng, 2017; Li et al., 2017). The slab-derived fluids would deliver soluble components of subducted carbonates and deliver them into the mantle source, resulting in the light Mg isotopes (Shen et al., 2018; Tian et al., 2018; Chen et al., 2021), as the unmodified mantle has a homogeneous $\delta^{26}Mg$ of -0.25 ± 0.04‰ (Teng et al., 2010). Previous studies suggest that the mantle source of the Xiarihamu Ni-Cu deposit experienced metasomatism by subduction-related fluids, as the evidence of high Ba/Th ratios (12.3–453.6) and low $(Ta/La)_N$ ratios (0.06–0.55) (Jiang et al., 2015; Peng et al., 2016; Jia et al., 2021), giving rise to the oxidized primitive magma of the Xiarihamu ultramafic intrusion. The whole-rock $\varepsilon_{Nd}(t)$ values of the Shitoukengde intrusion are higher than those of the Xiarihamu ultramafic rocks (-4.46–2.83 and -7.59–-0.74, respectively, Jia et al., 2021; Jiang et al., 2015; Peng et al., 2016), consistent with the mantle source of the former having experienced weaker metasomatism than the latter. This is also supported by the lower Ba/Th ratios (14.9–219.2) and higher $(Ta/La)_N$ ratios (0.54–2.84) of the Shitoukengde ultramafic rocks (Jia et al., 2021). Therefore, the degree of metasomatism of the mantle source may be the most convincing reason for the different primitive magma fO_2 of two coeval mafic-ultramafic intrusions in East Kunlun. Oxidation of the mantle source by metasomatism converts some sulfide into sulfate, which would increase the solubility of sulfur and chalcophile elements in the primitive magma (Mungall, 2002; Tomkins et al., 2012), and provide for higher concentrations of ore-forming components in the magmatic precursors to the Xiarihamu Ni-Cu deposit.

The most striking feature between the Xiarihamu and Shitoukengde intrusions is their different evolution trends of oxygen fugacity during magma emplacement at the shallow crustal level (Fig. 6). Crustal sulfur contamination is crucial for most magmatic Ni-Cu ore deposits (e.g., Holwell et al., 2007; Lesher and Barnes, 2008; Keays and Lightfoot, 2010; Fiorentini et al., 2012; Ripley and Li, 2017). The country gneisses of the Xiarihamu ore-bearing bodies contain considerable sulfide (Supplemental Figs. S2a-b), with whole-rock S contents reaching up to 1.14 wt.%. The in-situ $\delta^{34}S$ values of the Xiarihamu sulfide ores range from 2.4 to 7.7‰ (Li et al., 2015; Liu et al., 2018) and fall between those of the country gneiss (11.2‰, Liu et al., 2018) and mantle (0±2‰, Chaussidon et al., 1989), permitting the gneisses to have contributed S in the formation of the Xiarihamu sulfide ores. In addition, the $\delta^{26}Mg$ values of orthopyroxene increased progressively from harzburgites to websterites and gabbronorites (-0.49 to -0.21‰, Chen et al., 2021), which was interpreted to be due to variable degrees of crustal contamination (Brewer et al., 2018). Therefore, the oxidized primitive magma of the Xiarihamu deposit gradually became reduced with continuous addition of the external reduced sulfur from the country gneisses during emplacement, which lowered the sulfur solubility of the magma, causing S saturation and precipitation of sulfides to form the Xiarihamu Ni-Cu deposit. Coincidentally, previous studies suggested that the Ni-Cu deposits (e.g., Poyi, Huangshannan) in the

Central Asian Orogenic Belt (Zhang et al., 2009a, 2009b; Mao et al., 2018; Xue et al., 2021) could also be result from a relatively oxidized mantle source that gradually became more reduced during crustal processes (Fig. 6a). The mineralization process of the Xiarihamu Ni-Cu deposit was also documented by sulfide microtextures. Sulfides commonly occur as interstitial phases in the matrix (Figs. 3a, b, e), suggesting they crystallized after olivine and orthopyroxene. This could be the result of the decreasing fO_2 which was caused by the input of external sulfur during late magmatic evolution.

Although the country rocks of the Shitoukengde intrusion are also granitic gneisses, no sulfides were observed in thin sections (Supplemental Figs. S2c-d). Their whole-rock S contents (0.005–0.018 wt.%) are significantly lower than those of the Xiarihamu granitic gneisses (1.08–1.14 wt.%). Therefore, crustal sulfur contamination was likely very limited in the Shitoukengde intrusion. In this regard, the observed increase in magma fO_2, as shown in Fig. 6b, may have instead been driven by fractional crystallization. Previous studies have shown limited increases in $Fe^{3+}/\Sigma Fe$ ratios with the crystallization of olivine and pyroxenes, which cannot significantly change the magma oxygen fugacity (Cottrell and Kelley, 2011; Crabtree and Lange, 2012; Kelley and Cottrell, 2012). However, the FeO contents of Cr-spinel increase with decreasing olivine Fo values, suggesting that the crystallization of Cr-spinel would have depleted the FeO in liquid if the magma was a closed system (Cottrell and Kelley, 2011; Wykes et al., 2015). Our data show that the $Fe^{3+}/\Sigma Fe$ ratio increases with increasing FeO contents in Cr-spinel (Fig. 7), suggesting that the Shitoukengde magma fO_2 likely increased with the fractional crystallization of large amounts of Cr-spinel. The increase of oxygen fugacity during crystallization, as well as lack of crustal sulfur contamination, probably hampered the formation of sulfide ores in the Shitoukengde intrusion.

6.4 A genetic model for the mafic-ultramafic intrusions and the related Ni-Cu deposits in East Kunlun

Magmatic oxygen fugacity of Ni-Cu sulfide deposits has been studied extensively for decades but remains controversial (Mungall et al., 2006; Thakurta et al., 2008; Tomkins et al., 2012; Jugo, 2009; Brenan and Caciagli, 2000; Ballhaus et al., 1991). For example, the Voisey's Bay Cu-Ni deposit formed in a reduced environment (Brenan and Caciagli, 2000; Tomkins et al., 2012), but the Mirabela deposit formed in a relatively oxidized magma (Barnes et al., 2013). A likely contributor to this controversy is the impact of the different oxybarometers used, which reflect different redox states in the magmatic evolution process. For example, the magma fO_2 of the Huangshandong and Huangshanxi Cu-Ni deposits based on olivine-spinel pairs (ΔQFM+1–ΔQFM+2.6, Cao et al., 2019) is higher than that calculated by olivine-sulfide pairs (ΔQFM-1–ΔQFM+1, Mao et al., 2018), which may represent the fO_2 of the magmas before sulfide saturation and concurrent with sulfide saturation, respectively. A genetic model of the second largest Ni-Cu deposit and other comparable intrusions in China is built to reveal the relationship of magma fO_2 and Ni-Cu sulfide deposits.

The ophiolite fragments (e.g., Heishan and Qingshuiquan) in East Kunlun preserve a record of Proto-Tethys Ocean formed in the Early Paleozoic (Jiang et al., 1992; Yang et al., 1996; Cui et al., 2011; Meng et al., 2015). The Huxiaoqin mafic rocks (438 Ma, Liu et al., 2013a) and Qingshuiquan diabase-dikes (436 Ma, Ren et al., 2009) may represent the latest magmatism related to the Early Paleozoic ocean subduction (Liu et al., 2013b). The Wenquan eclogite with the peak metamorphic age of ~428 Ma in East Kunlun suggests a deep subduction during continent-continent collision (Meng et al., 2013b; Jia et al., 2014). After 428 Ma, extensive Silurian basalts (428–419 Ma, Zhu et al. 2006) and Early Devonian-Middle Devonian mafic dikes (412–383 Ma, Sun et al. 2004; Zhang et al. 2013; Xiong et al., 2014; Yang et al. 2014) in the East Kunlun area intruded, which represent the product of an extensional environment (Liu et al. 2013b; Peng et al. 2016; Song et al. 2016; Zhang et al. 2018). Therefore, the Xiarihamu and Shitoukengde intrusions (420–424 Ma) were emplaced in a post-collisional setting (Jia et al., 2021).

During this period, the cessation of subduction may cause break-off of the dense subducted slab, triggering upwelling of the hot asthenosphere mantle (Peng et al., 2016; Liu et al., 2018; Jia et al., 2021). The subducted slab experienced metamorphic dehydration and partial melting, and produced subduction-related aqueous fluids and hydrous melts (Zhao et al., 2007; Zheng, 2012), which metasomatized the overlying lithospheric and/or depleted asthenosphere mantle (Fig. 8a). Previous studies have suggested that metasomatic enrichment would increase the oxygen fugacity of the mantle wedge (McCammon et al., 2001; Creighton et al., 2008), which produced relatively oxidized primary magma. With the proceeding of emplacement, the magma became reduced progressively due to contamination of the external reduced crustal sulfur, which directly led to S saturation and sulfide segregation. The sulfide-loaded magmas produced the Xiarihamu deposit, with gradually decreasing magma fO_2 (Fig. 8b, ΔQFM+2.2±1.0 to ΔQFM-0.6±0.2).

The Shitoukengde intrusion in East Kunlun probably belongs to a different system comparing to the Xiarihamu Ni-Cu deposit. Without metasomatism of the subduction-related fluids, a relatively low-fO_2 primitive magma was generated in a mantle source with a limited capacity to dissolve sulfur. Fractional crystallization of a large amount of Cr-spinel elevated the magma fO_2, while there was no supplement of external reduced materials. The insufficient contents of sulfur in the primitive magma, coupled with increasing sulfur solubility of the magma caused by elevated fO_2 during crystallization, hampered sulfide precipitation in the Shitoukengde mafic-ultramafic intrusion.

7 Implications

Our study presents the first comparison of the magma fO_2 calculated by olivine-spinel oxybarometry for the Xiarihamu Ni-Cu sulfide deposit and Shitoukengde mafic-ultramafic intrusion in East Kunlun, and provides new insights into the relationship between magmatic oxygen fugacity and Ni-Cu mineralization. The second standard calibration method can effectively improve the accuracy of the Cr-spinel $Fe^{3+}/\Sigma Fe$ ratios by EPMA. A strong positive correlation is displayed between the magma fO_2 and Cr-spinel $Fe^{3+}/\Sigma Fe$ ratios, indicating that Cr-spinel $Fe^{3+}/\Sigma Fe$ ratios can be used as an indicator of magma fO_2. The evolution trend of the magma fO_2, from ΔQFM+2.2±1.0 to ΔQFM-0.6±0.2 with decreasing olivine Fo values, can reasonably explain the metallogenesis of the Xiarihamu deposit. Metasomatism happened in the mantle source by subduction-related fluid, generating the oxidized primary magmas, capable to transporting sulfur efficiently. Addition of external reduced sulfur from gneisses country rocks (1.08–1.14 wt.% S) during crustal processes led to deposition of sulfides and formation of the Xiarihamu Ni-Cu deposit.

Conversely, the Cr-spinel $Fe^{3+}/\Sigma Fe$ ratios of the Shitoukengde intrusion increase from 0.07±0.02 to 0.23±0.04, corresponding to fO_2 varying from ΔQFM-1.3±0.3 to ΔQFM+1.0±0.5. The fractional crystallization of large amounts of Cr-spinel can reasonably explain the increasing magma fO_2 during magmatic evolution, which would hamper sulfide precipitation in the Shitoukengde intrusion.

As a consequence, reduction processes of the oxidized primitive magma from mantle source to shallow crust are crucial for the Ni-Cu sulfide deposits. We propose that monitoring the temporal evolution of the magma fO_2 calculated by olivine-spinel oxybarometry can be a key indicator of metallogenic potential of Ni-Cu sulfide deposits.

Acknowledgments

The authors thank Dongyang Zhang and Baolong Li for the help with field work. We are grateful to Yadong Wu for providing spinel standard samples. We are also grateful to Prof. Paul Tomascak, Pedro Jugo, Christopher Jenkins, and an anonymous reviewer for their constructive suggestions and comments. This study was financially supported by the National Natural Science Foundation of China (No. 41822202, 42002096) and the Experimental Technology Innovation Fund of the Institute of Geology and Geophysics, Chinese Academy of Sciences (No. 11990860).

References

Ahmed, A.H., Helmy, H.M., Arai, S., and Yoshikawa, M. (2008) Magmatic unmixing in spinel from late Precambrian concentrically-zoned mafic-ultramafic intrusions, Eastern Desert, Egypt. Lithos, 104, 85–98.

Armstrong, J.T. (1995) Citzaf-a package of correction programs for the quantitative electron microbeam X-ray-analysis of thick polished materials, thin-films, and particles. Microbeam Analasis, 4(3), 177–200.

Ballaus, C., Berry, R.F., and Green, D.H. (1991) High pressure experimental calibration of the olivine-orthopyroxene-spinel oxygen geobarometer: implications for the oxidation state of the upper mantle. Contributions to Mineralogy and Petrology, 107, 27–40.

Barnes, S.J., Roeder, and P.L. (2001) The Range of Spinel Compositions in Terrestrial Mafic and Ultramafic Rocks. Journal of Petrology, 42, 2279–2302.

Barnes, S.J., Godel, B., Gurer, D., Brenan, J.M., Robertson, J., and Paterson, D. (2013) Sulfide-Olivine Fe-Ni Exchange and the Origin of Anomalously Ni Rich Magmatic Sulfides. Economic Geology, 108, 1971–1982.

Berry, A.J., Stewart, G.A., O'Neill, H.S.C., Mallmann, G., and Mosselmans, J.F.W. (2018) A re-assessment of the oxidation state of iron in MORB glasses. Earth and Planetary Science Letters, 483, 114–123.

Bian, Q.T., Li, D.H., Pospelov, I., Yin, L.M., Li, H.S., Zhao, D.S., Chang, C.F., Luo, X.Q., Gao, S.L., Astrakhantsev, O., and Chamov, N. (2004) Age, geochemistry and tectonic setting of Buqingshan ophiolites, north Qinghai-Tibet Plateau, China. Journal of Asian Earth Sciences, 23(4), 577–596.

Birner, S.K., Warren, J.M., Cottrell, E., and Davis, F.A. (2016) Hydrothermal alteration of seafloor peridotites does not influence oxygen fugacity recorded by spinel oxybarometry. Geology, 44, 535–538.

Birner, S.K., Cottrell, E., Warren, J.M., Kelley, K.A., Davis, F.A. (2018) Peridotites and basalts reveal broad congruence between two independent records of mantle fO_2 despite local redox heterogeneity. Earth and Planetary Science Letters, 494, 172–189.

Brandon, A.D., and Draper, D.S. (1996) Constaints on the origin of the oxidation state of mantle overlying subduction zones: An example from Simcoe, Washington, USA. Geochimica et Cosmochimica Acta, 60(10), 1739–1749.

Brenan, J.M., and Caciagli, N.C. (2000) Fe-Ni exchange between olivine and sulphide liquid: Implications for oxygen barometry in sulphide-saturated magmas. Geochimica et Cosmochimica Acta, 64, 307–320.

Brewer, A.W., Teng, F.Z., andMullen, E. (2018) Magnesium isotopes as a tracer of crustal materials in volcanic arc magmas in the northern Cascade Arc. Frontiers in Earth Science 6, 21, doi: 10.3389/feart.2018.00021.

Bryndzia, L.T., and Wood, B.J. (1990) Oxygen thermobarometry of abyssal spinel peridotites: the redox state and C–O–H volatile composition of the Earth's sub-oceanic upper mantle. American Journal of Science, 290(10), 1093–1116.

Brounce, M.N., Kelley, K.A., and Cottrell, E. (2014) Variations in $Fe^{3+}/\sum Fe$ of mariana arc basalts and mantle wedge fO_2. Journal of Petrology, 55, 2513–2536.

Bucholz, C.E., and Kelemen, P.B. (2019) Oxygen fugacity at the base of the Talkeetna arc, Alaska. Contributions to Mineralogy and Petrology 174, 79, https://doi.org/10.1007/s00410-019-1609-z

Candia, M.A.F., and Gaspar, J.C. (1997) Chromian spinels in metamorphosed ultramafic rocks from Mangabal I and II complexes, Goias, Brazil. Mineralogy and Petrology, 60, 27–40.

Canil, D.O, and Neill, H.S.C. (1996) Distribution of ferric iron in some upper-mantle assemblages. Journal of Petrology, 37, 609–35.

Cao, Y.H., Wang, Y.C., and Wei, B. (2019) Magma oxygen fugacity of Permian to Triassic Ni-Cu sulfide-berading mafic-ultramafic intrusions in the central Asian orogenic belt, North China. Journal of Asian Earth Sciences, 173, 250–262.

Carroll, M.R., and Rutherford, M.J. (1987) The stability of igneous anhydrite—Experimental results and implications for sulfur behavior in the 1982 El Chichon trachyandesite and other evolved magmas: Journal of Petrology, 28, 781–801.

Carroll, M.R., and Rutherford, M.J. (1988) Sulfur speciation in hydrous experimental glasses of varying oxidation state: Results from measured wavelength shifts of sulfur X-rays. American Mineralogist, 83, 845–849.

Chaussidon, M., Albarede, F., and Sheppard, S.M.F. (1989) Sulfur isotope heterogeneity in the mantle from ion microprobe measurements of sulfide inclusions in diamonds. Nature, 330, 242–244.

Chen, H.W., Luo, Z.H., Mo, X.X., Zhang, X.T., Wang , J., and Wang, B.Z. (2006c) SHRIMP ages of Kayakedengtage complex in the East Kunlun Mountains and their geological implications. Acta Petrologica et Mineralogica, 25(1), 25–32.

Chen, L., Sun, Y., Pei, X.Z.,Gao, M., Feng, T., Zhang, Z.Q., and Chen, W. (2001) Northernmost paleo-tethyan oceanic basin in Tibet: geochronological evidence from $^{40}Ar/^{39}Ar$ age dating of Dur'ngoi ophiolite. Chinese Science Bulletin, 46, 1203–1205.

Chen, L.M., Song, X.Y., Hu, R.Z., Yu, S.Y., Yi, J.N., Kang, J., and Huang, K.J. (2021) Mg-Sr-Nd Isotopic Insights into Petrogenesis of the Xiarihamu Mafic-ultramafic Intrusion, Northern Tibetan Plateau, China. Journal of Petrology, 1–25, doi: 10.1093/petrology/egaa113.

Chen, N.S., Li, X.Y., Wang, X.Y., Chen, Q., Wang, Q.Y., and Wan, Y.S. (2006a) Zircon SHRIMP U–Pb age of Neoproterozoic metagranite in the North Kunlun unit on the southern margin of the Qaidam block in China. Geological Bulletin of China, 25 (11), 1311–1314 (in Chinese with English abstract).

Chen, N.S., Li, X.Y., Zhang, K.X., Wang, G.C., Zhu, Y.H., Hou, G.J., and Bai, Y.S. (2006b) Lithological characteristics of the Baishahe Formation south of Xiangride Town, Eastern Kunlun Mountains and its age constrained from zircon Pb–Pb dating. Geological Science and Technology Information, 25, 1–7 (in Chinese with English Abstract).

Chen, N.S., Sun, M., Wang, Q.Y., Zhao, G.C., Chen, Q., and Shu, G.M. (2007) EMP chemical ages of monazites from Central Zone of the eastern Kunlun Orogen: records of multi tectonometamorphic events. Chinese Science Bulletin, 52, 2252–2263.

Clemente, B., Scaillet, B., and Pichavant, M. (2004) The solubility of sulphur in rhyolitic melts. Journal of Petrology, 45, 2171–2196.

Cottrell, E., and Kelley, K.A. (2011) The oxidation state of Fe in MORB glasses and the oxygen fugacity of the upper mantle. Earth and Planetary Science Letters, 305, 270–282.

Crabtree, S.M., and Lange, R.A. (2012) An evaluation of the effect of degassing on the oxidation state of hydrous andesite and dacite magmas: a comparison of pre-and post-eruptive Fe^{2+} concentrations.

Contributions to Mineralogy and Petrology, 163, 209–224.

Creighton, S., Stachel, T., Matveev, S., Hofer, H., McCammon, C., and Luth, R.W. (2008) Oxidation of the Kaapvaal lithospheric mantle driven by metasomatism. Contribution of Mineralogy and Petrology, 157, 491–504.

Cui, M.H., Meng, F.C., and Wu, X.K. (2011) Early Ordovician island arc of Yaziquan, west of Qimantag Mountain, Eastern Kunlun: evidences from geochemistry, Sm–Nd isotopes and geochronology of intermediate-basic igneous rocks. Acta Petrologica Sinica, 27, 3365–3379 (in Chinese with English Abstract).

Davis, F.A., Cottrell, E., Birner, S.K., Warren, J.M., and Lopez, O.G. (2017) Revisiting the electron microprobe method of spinel-olivine-orthopyroxene oxybarometry applied to spinel peridotites. American Mineralogist, 102(2), 421–435.

Deng, Y.F., Song, X.Y., Hollings, P., Chen, L.M., Zhou, T.F., Yuan, F., Xie, W., Zhang, D.Y., and Zhao, B.B. (2017) Lithological and geochemical constraints on the magma conduit systems of the Huangshan Ni-Cu sulfide deposit, NW China. Miner Deposita, 52, 845–862.

Dyar, M.D., Agresti, D.G., Schaefer, M., Grant, C.A., and Sklute, E.C. (2006) Mössbauer spectroscopy of earth and planetary materials. Annual Reviews of Earth and Planetary Science, 34, 83–125.

Evans, K.A., and Tomkins, A. (2011) The relationship between subduction zone redox budget and arc magma fertility: Earth and Planetary Science Letters, 308, 401–409.

Evans, K.A. (2012) The redox budget of subduction zones. Earth Science Reviews, 113, 11–32.

Enders, M., Speer, D., Maresch, W.V., and McCammon, C.A. (2000) Ferric/ferrous iron ratios in sodic amphiboles: Mossbauer analysis, stoichiometry-based model calculations and the high-resolution microanalytical flank method. Contributions to Mineralogy and Petrology, 140(2), 135–147.

Feng, C.Y., Qu, W.J., Zhang, D.Q., Dang, X.Y., Du, A.D., Li, D.X., and She, H.Q. (2009) Re-Os dating of pyrite from the Tuolugou stratabound Co(Au) deposit, eastern Kunlun Orogenic Belt, northwestern China. Ore Geology Reviews, 36, 213–220.

Feng, C.Y., Zhao, Y.M., Li, D.X., Liu, J.N., and Liu, C.Z. (2016) Mineralogical Characteristics of the Xiarihamu Nickel Deposit in the Qiman Tagh Mountain, East Kunlun, China. Geological Review, 62(1), 215–228 (in Chinese with English abstract).

Feng, J.Y., Pei, X.Z., Yu, S.L., Ding, S.P., Li, R.B., Sun, Y., Zhang, Y.F., Li, Z.C., Chen, Y.X., Zhang, X.F., and Chen, G.C. (2010) The discovery of the mafic-ultramafic mélange in Kekesha area of Dulan County, East Kunlun region, and its LA-ICP-MS zircon U-Pb age. Geology in China, 37(1), 28–38 (in Chinese with English abstract).

Fiorentini, M.L., Bekker, A., Rouxel, O., Wing, B.A., Maier, W., and Rumble, D. (2012) Multiple sulfur and iron isotope composition of magmatic Ni-Cu-(PGE) sulfide mineralization from eastern Botswana: Economic Geology, 107, 105–116.

Gaborieau, M., Laubier, M., Casanova, N.B., McCammon, C.A., Vantelon, D., Chumakov, A.I., Schiavi, F., Neuville, D.R., and Venugopal, S. (2020) Determination of $Fe^{3+}/\sum Fe$ of olivine-hosted melt inclusions using Mossbauer and XANES spectroscopy. Chemical Geology, 547, 11946.

Goldschmidt, V. M. (1937) The principles of distribution of chemical elements in minerals and rocks. Journal of the Chemical Society, 655–673.

Henderson, P., and Wood, R.J. (1981) Reaction relationships of chrome-spinels in igneous rocks – further evidence from the layered intrusion of Rhum and Mull, Inner Hebrides, Scotland. Contributions to Mineralogy and Petrology, 78, 225–229.

Höfer, H.E., Weinbruch, S., McCammon, C.A., and Brey, G.P. (2000) Comparison of two electron probe microanalysis techniques to determine ferric iron in synthetic wüstite samples. European Journal of Mineralogy, 12(1), 63–71.

Holwell, D.A., Boyce, A.J., and McDonald, I. (2007) Sulfur isotope variations within the Platreef Ni-Cu-PGE deposit: Genetic implications for the origin of sulfide mineralization. Economic Geology, 102, 1091–1110.

Hou, T., Botcharnikov, R., Moulas, E., Just, T., Berndt, J., Koepke, J., Zhang, Z.C., Wang, M., Yang, Z.P., Holtz, F. (2021) Kinetics of Fe-Ti Oxide Re-equilibration in Magmatic Systems: Implications for Thermo-oxymetry. Journal of Petrology, 1-24, doi: 10.1093/petrology/egaa116

Imai, A., Listanco, E.L., and Fujii, T. (1993) Petrologic and sulfur isotopic significance of highly oxidized and sulfur-rich magma of Mt. Pinatubo, Philippines. Geology, 21, 699–702.

Irvine, T.N. (1965) Chromian spinel as a petrogenetic indicator. Part I. Theory. Canadian Journal of Earth Sciences, 2 (6), 648–672.

Jenner, F. E., O'Neill, H. S. C., Arculus, R. J., and Mavrogenes, J. A. (2010) The magnetite crisis in the evolution of arc-related magmas and the initial concentration of Au, Ag and Cu. Journal of Petrology, 51, 2445–2464.

Jia, L.H., Meng, F.C., and Feng, H.B. (2014) Fluid activity during eclogite-facies peak metamorphism: Evidence from a quartz vein in eclogite in the East Kunlun, NW China. Acta Petrologica Sinica, 30(8), 2339–2350 (in Chinese with English abstract).

Jia, L.H., Meng, F.C., and Feng, H.B. (2018) The Wenquan ultramafic rocks in the Central East Kunlun Fault zone, Qinghai-Tibet Plateau—crustal relics of the Paleo-Tethys ocean. Mineralogy and Petrology, 112, 317–339.

Jia, L.H., Mao, J.W., Li, B.L., Zhang, D.Y., and Sun, T.T. (2021) Geochronology and petrogenesis of the

Late Silurian Shitoukengde mafic–ultramafic intrusion, NW China: Implications for the tectonic setting and magmatic Ni-Cu mineralization in the East Kunlun Orogenic Belt. International Geology Review, 63, 549–570.

Jiang, C.F., Yang, J.S., Feng, B.G., Zhu, Z.Z., Zhao, M., and Chai, Y.C. (1992) Opening-Closing Tectonics of Kunlun Mountains. Beijing: Geological Publishing House, 1–224 (in Chinese with English abstract).

Jiang, C.Y., Ling, J.L., Zhou, W., Du, W., Wang, Z.X., Fan, Y.Z., Song, Y.F., and Song, Z.B. (2015) Petrogenesis of the Xiarihamu Ni-bearing layered mafic-ultramafic intrusion, East Kunlun: Implications for its extensional island arc environment. Acta Petrologica Sinica, 31(4), 1117–1136 (in Chinese with English abstract).

Jugo, P.J. (2009) Sulfur content at sulfide saturation in oxidized magmas. Geology, 37(5), 415–418.

Jugo, P.J., Wilke, M., and Botcharnikov, R.E. (2010) Sulfur K-edge XANES analysis of natural and synthetic basaltic glasses: Implications for S speciation and S content as function of oxygen fugacity. Geochimica et Cosmochimica Acta, 74(20), 5926–5938.

Kamenetsky, V.S., Crawford, A.J., and Meffre, S. (2001) Factors controlling chemistry of magmatic spinel: an empirical study of associated olivine, Cr-spinel and melt inclusions from primitive rocks. Journal of Petrology, 42, 655–671.

Keays, R.R., and Lightfoot, P.C. (2010) Crustal sulfur is required to form magmatic Ni-Cu sulfide deposits: evidence from chalcophile element signatures of Siberian and Deccan Trap basalts. Mineralium Deposita, 45, 241–257.

Kelley, K.A., and Cottrell, E. (2012) The influence of magmatic differentiation on the oxidation state of Fe in a basaltic arc magma. Earth and Planetary Science Letters 329, 109–121.

Kiseeva, E. S., Fonseca, R. O. C., and Smythe, D. J. (2017) Chalcophile elements and sulfides in the upper mantle. Elements, 13, 111–116.

Lee, C.T.A., Leeman, W.P., Canil, D., and Li, Z.X.A. (2005) Similar V/Sc systematics in MORB and arc basalts: Implications for the oxygen fugacities of their mantle source regions. Journal of Petrology, 46(11), 2313–2336.

Lesher, C.M., and Barnes, S.J. (2008) Komatiite-associated Ni-Cu-PGE deposits, *in* Arndt, N.T., ed., Komatiites. Cambridge University Press, 295−327.

Li, C.S., and Ripley, E.M. (2009) New Developments in Magmatic Ni-Cu and PGE Deposits; Geological Publishing House, Beijing, 290.

Li, C.S., Zhang, Z.W., Li, W.Y., Wang, Y.L., Sun, T., and Ripley, E.M. (2015) Geochronology, petrology and Hf-S isotope geochemistry of the newly-discovered Xiarihamu magmatic Ni-Cu sulfide deposit in the Qinghai-Tibet plateau, western China. Lithos, 216–217, 224–240.

Li, H.K., Lu, S.N., Xiang, Z.Q., Zhou, H.Y., Guo, H., Song, B., Zheng, J.K., and Gu, Q. (2006) SHRIMP U-Pb zircon age of the granulite from the Qingshuiquan area, Central Eastern Kunlun Suture Zone. Earth Science Frontiers, 13(6), 311–321 (in Chinese with English abstract).

Li, L., Sun, F.Y., Li, B.L., Li, S.J., Chen, G.J., Wang, W., Yan, J.M., Zhao, T.F., Dong, J., and Zhang, D.X. (2018) Geochronology, Geochemistry and Sr-Nd-Pb-Hf Isotopes of No. I Complex from the Shitoukengde Ni–Cu Sulfide Deposit in the Eastern Kunlun Orogen, Western China: Implications for the Magmatic Source, Geodynamic Setting and Genesis. Acta Geologica Sinica (English Edition), 92, 106–126.

Li, J.P., Kornprobst, J., and Vielzeuf, D. (1995) An improved experimental calibration of the olivine-spinel geothermomemter. Chinese Journal of Geochemistry, 14(1), 68–77.

Li, S.G., Yang, W., Ke, S., Meng, X., Tian, H., Xu, L., He, Y., Huang, J., Wang, X.C., Xia, Q., Sun, W., Yang, X., Ren, Z.Y., Wei, H., Liu, Y., Meng, F., Yan, J. (2017). Deep carbon cycles constrained by a large-scale mantle Mg isotope anomaly in eastern China. National Science Review 4, 111–120.

Lindsley, D.H., and Frost, B.R. (1992) Equilibria among Fe–Ti oxides, pyroxenes, olivine, and quartz: part I. Theory. American Mineralpgist, 77(9–10), 987–1003.

Liu, B., Ma, C.Q., Zhang, J.Y., Xiong, F.H., Huang, J., and Jiang, H.A. (2012) Petrogenesis of Early Devonian intrusive rocks in the east part of Eastern Kunlun Orogen and implication for Early Paleozoic orogenic processes. Acta Petrologica Sinica, 28, 1785–1807 (in Chinese with English abstract).

Liu, B., Ma, C.Q., Jiang, H.A., Guo, P., Zhang, J.Y., and Xiong, F.H. (2013a) Early Paleozoic tectonic transition from ocean subduction to collisional orogeny in the Eastern Kunlun region: evidence from Huxiaoqin mafic rocks. Acta Petrologica Sinica, 29 (6), 2093–2106 (in Chinese with English abstract).

Liu, B., Ma, C.Q., Pan, G., Zhang, J.Y., Xiong, F.H., Jian, H., and Jiang, H.A. (2013b) Discovery of the Middle Devonian A-type Granite from the Eastern Kunlun Orogen and Its Tectonic Implications. Earth Sciences (Journal of China Univiversity of Geoscienses), 38 (5), 947–962 (in Chinese with English abstract).

Liu, Y., Samaha, N.T., and Baker, D.R. (2007) Sulfur concentration at sulfide saturation (SCSS) in magmatic silicate melts. Geochimica et Cosmochimica Acta, 71, 1783–1799.

Liu, Y.G., Li, W.Y., Jia, Q.Z., Zhang, Z.W., Zhang, Z.A., Zhang, Z.B., Zhang, J.W., and Qian, B. (2018) The dynamic sulfide satration process and a possible slab break-off model for the giant Xiarihamu magmatic nickel ore deposit in the East Kunlun Orogenic Belt, Northern Qinghai-Tibet Plateau, China. Economic Geology, 113, 1383–1417.

Liu, Z.Q. (2011) Study on the Geological Characteristics and Tectonic of Buqingshan Melanges Belt, the South Margin of East Kunlun Mountains. Xi an：Chang An University (in Chinese with English abstract).

Liu, Z.Q., Pei, X.Z., Li, R.B., Li, Z.C., Zhang, X.F., Liu, Z.G., Chen, G.C., Chen, Y.X., Ding, S.P., and Guo, J.F. (2011) LA-ICP-MS zircon U-Pb geochronology of the two suites of ophiolite at the Buqingshan area of the A'nyemaqen orogenic belt in the southern margin of East Kunlun and its tectonic implication. Acta Geologica Sinica, 85, 185–194 (Chinese with English abstract)

Lu, S.N., Yu, H.F., Li, H.K., Guo, K.Y., Wang, H.C., Jin, W., Zhang, C.L., and Liu, Y.S. (2006) Research on Precambrian Major Problems in China: Precambrian Significant Geological Events in the Western China and Global Tectonic Implications. Geological Publishing House, Beijing 1–206 (in Chinese).

Lu, S.N., Li, H.K., Wang, H.C., Chen, Z.H., Zheng, J.K., and Xiang, Z.Q. (2009) Detrital zircon population of proterozoic metasedimentary strata in the Qinling–Qilian–Kunlun Orogen. Acta Petrologica Sinica, 25, 2195–2208 (in Chinese with English abstract).

Mao, Y.J., Qin, K.Z., Barnes, S.J., Tang, D.M., Xue, S.C., Le, V.M. (2017) Genesis of the Huangshannan high-Ni tenor magmatic sulfide deposit in the Easten Tianshan, northwest China: Constraints from PGE geochemistry and Os-S isotopes. Ore Geology Review, 90, 591–606.

Mao, Y.J., Qin, K.Z., Barnes, S.J., Ferraina, C., Marziano, G.I., Verrall, M., Tang, D.M., and Xue, S.C. (2018) A revised oxygen barometry in sulfide-saturated magmas and application to the Permian magmatic Ni-Cu deposits in the southern Central Asian Orogenic Belt. Miner Deposita, 53, 731–

755.

Matjuschkin, V., Blundy, J.D., and Brooker, R.R. (2016) The effect of pressure on sulphur speciation in mid- to deep-crustal arc magmas and implications for the formation of porphyry copper deposits. Contributions to Mineralogy and Petrology, 171, 66.

Mavrogenes, J.A., and O'neill, H.S.C. (1999) The relative effects of pressure, temperature and oxygen fugacity on the solubility of sulfide in mafic magmas. Geochimica et Cosmochimica Acta, 63(7/8), 1173–1180.

McCammon, C.A., Griffin, W.L., Shee, S.R., and O'Neill, H.S.C. (2001) Oxidation during metasomatism in ultramafic xenoliths from the Wesselton kimberlite, South Africa: implications for the survival of diamond. Contribution of Mineralogy and Petrology, 141, 287–296.

McCammon, C.A., McEnroe, S.A., Robinson, P., Fabian, K., and Burton, B.P. (2009) High efficiency of natural lamellar remanent magnetization in single grains of ilmeno-hematite calculated using Mossbauer spectroscopy. Earth and Planetary Science Letters, 288, 268–278.

Meng, F.C., Cui, M.H., Wu, X.K., Wu, J.F., and Wang, J.H. (2013a) Magmatic and metamorphic events recorded in granitic gneisses from Qimantag, East Kunlun Mountains, Northwest China. Acta Petrologica Sinica, 29, 2107–2122 (in Chinese with English abstract).

Meng, F.C., Zhang, J.X., and Cui, M.H. (2013b) Discovery of Early Paleozoic eclogite from the East Kunlun, Western China and its Tectonic significance. Gondwana Research, 23(2), 825–836.

Meng, F.C., Cui, M.H., Wu, X.K., and Ren, Y.F. (2015) Heishan mafic-ultramafic rocks in the Qimantag area of Eastern Kunlun, NW China: Remnants of an early Paleozoic incipient island arc. Gondwana Research, 27, 745–759.

Mo, X.X., Luo, Z.H., Deng, J.F., Yu, X.H., Liu, C.D., Zhan, H.W., Yuan, W.M., and Liu, Y.H. (2007).

Granitoids and crustal growth in the East-Kunlun orogenic belt. Geological Journal of China University, 13(3), 403–414 (Chinese with English abstract)

Moussallam, Y., Edmonds, M., Scaillet, B., Peters, N., Gennaro, E., Sides, I., and Oppenheimer, C. (2016) The impact of degassing on the oxidation state of basaltic magmas: A case study of Kilauea volcano. Earth and Planetary Science Letters, 450, 317–325.

Mukherjee, R., Mondal, S.K., Rosing, M.T., and Frei, R. (2010) Compositional variations in the Mesoarchean chromites of the Nuggihalli schist belt, Western Dharwar Craton (India): potential parentalmelts and implications for tectonic setting. Contributions to Mineralogy and Petrology, 160, 865–885.

Mungall, J. E. (2002) Roasting the mantle: Slab melting and the genesis of major Au and Au-rich Cu deposits. Geology, 30, 915–918.

Mungall, J.E., Andrews, D.R.A., Cabri, L., Sylvester, P.L., and Tubrett, M. (2005) Partitioning of Cu, Ni, Au and platinum-group elements between monosulfide solid solution and sulfidemelt under controlled oxygen and sulfur fugacities. Geochim Cosmochim Acta, 69, 4349–4360.

Mungall, J.E., Hanley, J.J., Arndt, N.T., and Debecdelievre, A. (2006) Evidence from meimechites and other low-degree mantle melts for redox contrals on mantle-crust fractionation of platinum-group elements. Proceedings of the National Academy of Sciences of the United States of America, 103, 12695–12700.

Mysen, B.O., Carmichael, I.S.E., and Virgo, D. (1985) A comparison of iron redox ratios in silicate glasses determined by wet-chemical and ^{57}Fe Mössbauer resonant absorption methods. Contributions to Mineralogy and Petrology, 90, 101–106.

Naldrett, A. J. (2004) Magmatic Sulfide Deposits: Geology, Geochemistry, and Exploration. Berlin:

Springer.

Naldrett, A.J. (2011) Fundamentals of magmatic sulfide deposits. Reviews in Economic Geology, 17. 1–50.

Peng, B., Sun, F.Y., Li, B.L., Wang, G., Li, S.J., Zhao, T.F., Li, L., and Zhi, Y.B. (2016) The geochemistry and geochronology of the Xiarihamu II mafic-ultramafic complex, Eastern Kunlun, Qinghai Province, China: Implications for the genesis of magmatic Ni-Cu sulfide deposits. Ore Geology Reviews, 73, 13–28.

Qi, S.S. (2015) Petrotectonic assemblages and tectonic evolution of the East Kunlun orogenic belt in Qinghai Province. China University of Geosciences, Wuhan.

Qi, S.S., Song, S.G., Shi, L.C., Cai, H.J., and Hu, J.C. (2014) Discovery and its geological significance of Early Paleozoic eclogite in Xiarihahu–Suhaitu area, western part of the East Kunlun. Acta Petrologica Sinica, 30, 3345–3356 (in Chinese with English abstract).

Qi, X.P., Yang, Jie., Fan, X.G., Cui, J.T., Cai, Z.F., Zeng, X.W., Wei, W., Qu, X.X., and Zhai, L.M. (2016) Age, geochemical characteristics and tectonic significance of Changshishan ophiolite in central East Kunlun tectonic mélange belt along the east section of East Kunlun Mountains. Geology in China, 43(3), 797–816 (in Chinese with English abstract).

Ren, J.H., Liu, Y.Q., Feng, Q., Han, W.Z., Gao, H., and Zhou, D.W. (2009) LA-ICP-MS U-Pb zircon dating and geochemical characteristics of diabase-dykes from the Qingshuiquan area, eastern Kunlun orogenic belt. Acta Petrologica Sinica, 25(5), 1135–1145.

Ripley, E.M., and Li, C.S. (2017) A review of the application of multiple S isotopes to magmatic Ni-Cu-PGE deposits and the significance of spatially variable $\triangle^{33}$S values. Economic Geology, 112, 983–991.

Roeder, P.L., and Campbell, I.H. (1985) The effect of postcumulus reactions on composition of chrome-spinels from the Jimberlana intrusion. Journal of Petrology, 26(3):763–786.

Shen, J., Li, S.G., Wang, S.J., Teng, F.Z., Li, Q.L., Liu, Y.S. (2018) Subducted Mg-rich carbonates into the deep mantle wedge. Earth and Planetary Science Letters 503, 118–130.

Sillitoe, R.H. (1997) Characteristics and controls of the largest porphyry copper-gold and epithermal gold deposits in the circum-Pacific region: Australian Journal of Earth Sciences, 44, 373–388.

Song, X.Y., Yi, J.N., Chen, L.M., She, Y.W., Liu, C.Z., Dang, X.Y., Yang, Q.A., and Wu, S.K. (2016) The Giant Xiarihamu Ni-Co Sulfide Deposit in the East Kunlun Orogenic Belt, Northern Tibet Plateau, China. Economic Geology, 111, 29–55.

Sun, W.D. (2020) Oxygen fugacity of Earth. Geochimica, 49(1), 1–20 (in Chinese with English abstract.).

Sun, Y., Zhang, G., Wang, J., Zhan, F., Zhang, Z. (2004) $^{40}Ar/^{39}Ar$ age of the basic sill swarms of two periods in the junctions area of Qinling and Kunlun and its tectonic significance. Acta Geologica Sinica, 78 (1), 65–71 (in Chinese with English abstract.).

Symonds, R.B., Rose, W.I., Bluth, G.J.S., and Gerlach, T.M. (1994) Volcanic gas studies—Methods, results, and applications: Volatiles in magmas: Reviews in Mineralogy, 30, 1–66.

Taranovic, V., Ripley, E.M., Li, C.S., and Rossell, D. (2016). Chalcophile element (Ni, Cu, PGE, and Au) variations in the Tamarack magmatic sulfide deposit in the Midcontinent Rift System: implications for dynamic ore-forming processes. Miner Deposita, 51, 937–951.

Tao, Y., Li, C.S., Song, X.Y., and Ripley, E.M. (2008) Mineralogical, petrological, and geochemical studies of the Limahe mafic–ultramatic intrusion and associated Ni–Cu sulfide ores, SW China. Miner Deposita, 43, 949–872.

Teng, F.Z. (2017). Magnesium isotope geochemistry. In: Teng, F.Z., Watkins, J. M., Dauphas, N. (eds) Non-traditional Stable Isotopes. Reviews in Mineralogy and Geochemistry, 82, 219–287.

Teng, F.Z, Li, W.Y., Ke, S., Marty, B., Dauphas, N., Huang, S., Wu, F.Y., Pourmand, A. (2010). Magnesium isotopic composition of the Earth and chondrites. Geochimica et Cosmochimica Acta, 74, 4150–4166.

Thakurta, J., Ripley, E.M., and Li, C. (2008) Geochemical constraints on the origin of sulfide mineralization in the Duke Island Complex, southeastern Alaska. Geochemistry, Geophysics, Geosystems 9, Q07003.

Tian, H.C., Yang, W., Li, S.G., Ke, S., Duan, X.Z. (2018) Low δ^{26}Mg volcanic rocks of Tengchong in Southwestern China: A deep carbon cycle induced by supercritical liquids. Geochimica et Cosmochimica Acta 240, 191–219.

Tomkins, A.G., Rebryna, K.C., Weinberg, R.F., and Schaefer, B.F. (2012) Magmatic sulfide formation by reduction of oxidized arc basalt. Journal of Petrology, 53(8), 1537–1567.

Wang, G. (2014) Metallogenesis of Nickel deposits in Eastern Kunlun Orogenic Belt [D], Qinghai Province. Jilin University, China (in Chinese with English abstract).

Wang, G., Sun, F.Y., Li, B.L., Li, S.J., Zhao, J.W., Ao, Z., and Yang, Q.A. (2014) Petrography, zircon U-Pb geochronology and geochemistry of the mafic-ultramafic intrusion in Xiarihamu Cu-Ni deposit from East Kunlun, with implications for geodynamic setting. Earth Science Frontiers, 21(06), 381–401 (in Chinese with English abstract).

Wang, G., Sun, F., Li, B., Ao, Z., Li, S., Zhao, J., and Yang, Q.A. (2016) Geochronology, geochemistry and tectonic implication of Early Neoproterozoic monzogranite in Xiarihamu ore district from East Kunlun: Geotectonica et Metallogenia, 40, 1247–1260 (in Chinese with English abstract).

Wang, G.C., Wang, Q.H., Jian, P., and Zhu, Y.H. (2004) Zircon SHRIMP ages of Precambrian metamorphic basement rocks and their tectonic significance in the eastern Kunlun Mountains, Qinghai Province, China. Earth Science Frontiers, 11(4), 481–490 (in Chinese with English abstract).

Wei, B. (2015) Study on the Geological Characteristic and Tectonic attribute of the Qphiolite and Island-arc-type Igneous Rocks, Central Belt of East Kunlun (Eastern Section). Chang'An University, Xi'an (in Chinese with English abstract)..

Wood, B.J., and Virgo, D. (1989) Upper mantle oxidation state: ferric iron contents of lherzolite spinels by ^{57}Fe Mossbauer spectroscopy and resultant oxygen fugacities. Geochim Cosmochim Acta, 53(6), 1277–1291.

Wood, B.J. (1990) An experimental test of the spinel peridotite oxygen barometer. Journal of Geophysical Research, 95, 15845–15851.

Wykes, J.L., O'Neill, H.S.C., and Mavrogenes, J.A. (2015) The effect of FeO on the sulfur content at sulfide saturation (SCSS) and the selenium content at selenide saturation of silicate melts: Journal of Petrology, 56, 1407–1424.

Xie, W., Song, X.Y., Chen, L.M., Deng, Y.F., Zheng, W.Q., Wang, Y.S., Ba, D.H., Yin, M.H., and Luan, Y. (2014) Geochemistry insights on the genesis of the subduction-related Heishan magmatic Ni-Cu-(PGE) deposit, Gansu, Northwestern China, at the Southern Margin of the Central Asian Orogenic Belt. Economic Geology, 109, 1563–1583.

Xu, Z.Q., Yang, J.S., Li, H.B., Zhang, J.X., and Wu, C.L. (2007) Orogenic Plateau: Terrane Amalgamation, Collision and Uplift in the Qinghai-Tibet Plateau. Beijing: Geological Publishing House, 1–458 (in Chinese with English abstract).

DOI: https://doi.org/10.2138/am-2022-8050. http://www.minsocam.org/

Xie, W., Song, X.Y., Deng, Y.F., Wang, Y.S., Ba, D.H., Zheng, W.Q., Li, X.B. (2014) Geochemistry and petrogenetic implications of a Late Devonian mafic-ultramafic intrusion at the soutthern margin of the Central Asian Orogenic Belt. Lithos 144, 209–230.

Xue, S.C., Qin, K.Z., Li, C.S., Tang, D.M., Mao, Y.J., Qi, L., Repley, E.M. (2016) Geochronological, petrological, and geochemical constraints on Ni-Cu sulfide mineralization in the Poyi ultramafic-troctolitic intrusion in the northeast rim of the Tarim craton, western China. Economy Geology 111, 1465–1484.

Xue, S.C., Deng, J., Wang, Q.F., Xie, W., Wang, Y.N. (2021) The redox conditions and C isotopes of magmatic Ni-Cu sulfide deposits in convergent tectonic settings: the role of reduction process in ore genesis. Geochimica et Cosmochimica Acta 306, 210–225.

Xiong, F.H., Ma, C.Q., Jiang, H., Liu, B., and Huang, J. (2014) Geochronology and geochemistry of Middle Devonian mafic dykes in the East Kunlun orogenic belt, northern Tibet plateau: Implications for the transition from Prototethys to Paleotethys orogeny. Chemie der Erde, 74, 225–235.

Yang, J.S., Robinson, P.T., Jiang, C.F., and Xu, Z.Q. (1996) Ophiolites of the Kunlun Mountains, China and their tectonic implications. Tectonophysics, 258(1–4), 215–231.

Yang, J.S.,Wang, X.B., Shi, R.D., Xu, Z.Q., and Wu, C.L. (2004) The Dur'ngoi ophiolite in East Kunlun, NE Tibetan plateau: a fragment of paleo-Tethyan oceanic lithosphere. Geology in China, 31, 225–239 (in Chinese with English abstract).

Yang, L., Zhou, H.W., Zhu, Y.H., Dai, X., Lin, Q.X., Ma, Z.Q., Jian, K.K., and Zhang, M.Y. (2014) Geochemical characteristics and LA-ICP-MS zircon U-Pb ages of intermediate to mafic dyke swarms in Haxiya area, Golmud, Qinghai Province. Geological Bulletin of China, 33 (6), 804–

819 (in Chinese with English abstract).

Yang, W., Teng, F.Z., Zhang, H.F., Li, S.G. (2012). Magnesium isotopic systematics of continental basalts from the North China craton: Implications for tracing subducted carbonate in the mantle. Chemical Geology, 328, 185–194.

Zhao, Z.F., Zheng, Y.F., Chen, R.X., Xia, Q.X., and Wu, Y.B. (2007) Element mobility in mafic and felsic ultrahigh-pressure metamorphic rocks during continental collision: Geochimica et Cosmochimica Acta, 71, 5244–5266.

Zhang, J.X., Meng, F.C., Wan, Y.S., Yang, J.S., and Tung, K.A. (2003) Early Paleozoic tectonothermal event of the Jinshuikou Group on the southern margin of Qaidam: zircon U–Pb SHRIMP age evidence. Geological Bulletin of China, 22, 397–404 (in Chinese with English abstract).

Zhang, J.X., Yu, S.Y., Li, Y.S., Yu, X.X., Lin, Y.H., and Mao, X.H. (2015) Subduction, accretion and closure of Proto-Tethyan Ocean: Early Paleozoic accretion/collision orogeny in the Altun-Qilian-North Qaidam orogenic system. Acta Petrologica Sinica, 31(12), 3531–3554 (in Chinese with English abstract).

Zhang, Z., Liu, L., Zhao, H., Zhou, Q., Tian, C., and Xu, B. (2013) Geological features and implication of mafic dykes swarm at northern Qimantag small basin in Qinghai. Journal of Qinghai University, 31 (4), 57–64 (in Chinese with English abstract).

Zhang, Z.C., Yan, S.H., Chen, B.L., Zhou, G., He, Y.K., Chai, F.M., He, L.X., and Wan, Y.S. (2006) SHRIMP zircon U-Pb dating for subduction-related granitic rocks in the northern part of east Junggar, Xinjiang. Chinese Science Bulletin, 51(8), 952–962.

Zhang, Z.C., Mao, J.W., Saunders, A.D., Ai, Y., Li, Y., and Zhao, L. (2009a) Petrogenetic modeling of three mafic-ultramafic layered intrusions in the Emeishan large igneous province, SW China, based on isotopic and bulk chemical constraints. Lithos, 113, 369–392.

Zhang, Z.C., Mao, J.W., Chai, F.M., Yan, S.H., Chen, B.L., and Pirajno, F. (2009b) Geochemistry of the Permian Kalatongke mafic intrusions, Northern Xinjiang, NW China, Implications for the Genesis of the Magmatic Ni-Cu Sulfide Deposit. Economic Geology, 104(2), 185–203.

Zhang, Z.W., Wang, Y.L., Qian, B., Liu, Y.G., Zhang, D.Y., Lu, P.R., and Dong, J. (2018) Metallogeny and tectonomagmatic setting of Ni-Cu magmatic sulfide mineralization, number I Shitoukengde mafic-ultramafic complex, East Kunlun Orogenic Belt, NW China. Ore Geology Reviews, 96, 236–246.

Zheng, Y.F. (2012) Metamorphic chemical geodynamics in continental subduction zones: Chemical Geology, 328, 5–48.

Zhou, W. (2016) Petrogenesis of Shitoukengde mafic-ultramafic intrusion and analysis of its metallogenic potential, East Kunlun. Xi an: Chang An University (in Chinese with English abstract).

Zhu, Y.H., Lin, Q.X., Jia, C.X., and Wang, G.C. (2005) SHRIMP zircon U–Pb age and significance of early Paleozoic volcanic rocks in the East Kunlun orogenic belt, Qinghai Province, China. Science in China (Series D), 49, 88–96 (in Chinese with English abstract).

Zhu, Y., Lin, Q., Jia, C., and Wang, G. (2006) SHRIMP zircon U-Pb age and significance of Early Paleozoic volcanic rocks in East Kunlun orogenic belt, Qinghai Province, China. Science in China (Series D: Earth Sciences), 49 (1), 88–96.

Figure captions

DOI: https://doi.org/10.2138/am-2022-8050. http://www.minsocam.org/

Fig. 1 (a) Tectonic sketch map of China; (b) Simplified tectonic units of the East Kunlun Orogenic Belt (modified after Feng et al., 2009 and Meng et al., 2015). (c) Simplified geologic map of the eastern portion of the East Kunlun Orogenic Belt (modified after Zhang et al., 2015). Zircon U-Pb geochronology data are listed in Supplemental Table S1.

Fig. 2 Geological map of the Xiarihamu I mafic-ultramafic intrusion (a) and cross-section (b) for the Xiarihamu magmatic sulfide deposit (modified after Song et al., 2016). (c) Simplified geological map of the Shitoukengde intrusion (modified after Jia et al., 2021). Zircon U–Pb age data of the Shitoukengde mafic-ultramafic rocks are from Zhou (2016), Li et al. (2018), Zhang et al. (2018).

Fig. 3 Photomicrographs in cross-polarized light and reflected light (b, d, j) and BSE images (h, n, o) of Cr-spinel characteristics from the Xiarihamu Ni-Cu deposit and Shitoukengde intrusion. **Xiarihamu**: (a-c) harzburgite; (d) lherzolite; (e) olivine orthopyroxenite; (f) websterite; (g) norite; **Shitoukengde**: (h) harzburgite; (i-j) lherzolite; (k) olivine websterite; (l) clinopyroxenite; (m) gabbro; (n-o) heterogeneous Cr-spinel grains. Mineral abbreviations: Ol olivine, Opx orthpyroxene, Cpx clinopyroxene, Pl plagioclase, Ts tschermakite, Spl Cr-spinel, Ap apatite, Sul sulfide, Po pyrrhotite, Pn pentlandite, Ccp chalcopyrite, Ilm ilmenite.

Fig. 4 Comparison of $Fe^{3+}/\Sigma Fe$ ratios measured by Mössbauer spectroscopy and EPMA modified by second standard calibration. The corrected $Fe^{3+}/\Sigma Fe$ ratios by EPMA are nearly identical to those by Mössbauer spectroscopy (Wood and Virgo, 1989). See text for details.

Fig. 5 Plots of $Fe^{3+}/\Sigma Fe$ ratios and log $fO_2(\Delta QFM)$ of Cr-spinels from the Xiarihamu Ni-Cu deposit. (a) and (b) show that $Fe^{3+}/\Sigma Fe$ ratios and log $fO_2(\Delta QFM)$ of Cr-spinel cores are slightly higher than those of Cr-spinel rims in different grains, (c) and (d) show that the $Fe^{3+}/\Sigma Fe$ ratios become lower from core to rim in individual Cr-spinel grain.

Fig. 6 Plots of oxygen fugacity shown as Fo values in olivine versus log $fO_2(\Delta QFM)$ for the Xiarihamu Ni-Cu deposit and Shitoukengde intrusion in East Kunlun, and several Ni-Cu deposits in Central Asian Orogenic Belt. (a) The most primitive magma of the Xiarihamu Ni-Cu deposit changed progressively from an oxidized to a reduced state, being reduced into the sulfide stability field, which would have caused sulfide segregation and ultimately ore deposit formation. Several typical Ni-Cu deposits in Central Asian Orogenic Belt also show a positive relation between magma fO_2 and olivine Fo values. (b) The most primitive magma fO_2 of the Shitoukengde intrusion was reduced and then became oxidized, which inhibited S saturation and sulfide segregation. Data source of Ol-Opx-Spl-Wood method: Huangshannan (HSN), Poyi (PY), Heishan (HS), and Xiarihamu (XRHM) from Xue et al. (2021); data source of Ol-Sul-Barnes method: HSN from Mao et al. (2017), PY from Xue et al. (2016), HS from Xie et al. (2014), and XRHM from Li et al. (2015).

Fig. 7 Plots of FeO concentration versus $Fe^{3+}/\Sigma Fe$ ratio in Cr-spinel for the Shitoukengde mafic-ultramafic intrusion. The trend line shows that the $Fe^{3+}/\Sigma Fe$ ratio increases with increasing FeO contents in Cr-spinel, suggesting that the Shitoukengde magma fO_2 likely increased with the fractional crystallization of large amounts of Cr-spinel.

DOI: https://doi.org/10.2138/am-2022-8050. http://www.minsocam.org/

Fig. 8 A genetic model for the Xiarihamu Ni-Cu deposit and Shitoukengde mafic-ultramafic intrusion in East Kunlun. See text for details.

Supplemental Fig. S1 The BSE images by TIMA of the Shitoukengde and Xiarihamu intrusions, showing the volume content of the Cr-spinel of the Shitoukengde (~2.32 vol.%) is higher than that of the Cr-spinel in the Xiarihamu lherzolite (~0.05 vol.%).

Supplemental Fig. S2 Photomicrographs images of country rocks from the Xiarihamu Ni-Cu deposit and Shitoukengde intrusion. Xiarihamu: a-Amphibole plagiogneiss; b-Amphibole plagiogneiss contains sulfide grain; Shitoukengde: c-Amphibole gneiss; d-Biotite plagiogneiss. Mineral abbreviations: Pl plagioclase, Amp amphibole, Bt biotite, Grt garnet, Qtz quartz, Sul sulfide.

Supplemental Fig. S3 Comparison of Cr-spinel $Fe^{3+}/\Sigma Fe$ ratios measured by Mössbauer spectroscopy and EPMA modified by second standard calibration, showing the reproducibility of this method.

Supplemental Fig. S4 Plots of Fo values in olivine versus $T_{Ol\text{-}Spl}$ (℃) for the Xiarihamu Ni-Cu deposit and Shitoukengde intrusion.

Supplemental Fig. S5 Correlation diagrams of (a) FeO in Cr-spinel and FeO in olivine and (b) MgO in Cr-spinel and MgO in olivine for the Shitoukengde intrusion. (c) and (d) show that the FeO contents become lower from core to rim in the individual Cr-spinel grain.

DOI: https://doi.org/10.2138/am-2022-8050. http://www.minsocam.org/

Supplemental Fig. S6 Correlation between log fO_2(ΔQFM) and Cr-spinel $Fe^{3+}/\Sigma Fe$ ratio, showing a strong positive correlation between the fO_2 and Cr-spinel $Fe^{3+}/\Sigma Fe$ ratios from the Xiarihamu Ni-Cu deposit and Shitoukengde mafic-ultarmafic intrusion.

Table captions

Supplemental Table S1

Summary of geochronology for the mafic-ultramafic intrusions and eclogites in the East Kunlun Orogenic belt.

Supplemental Table S2

Composition of Cr-spinel standards determined by EPMA, to test the reproducibility of the secondary standard calibration method.

Supplemental Table S3

Electron microprobe results (in wt.%) of the secondary Cr-spinel standard samples.

Supplemental Table S4

Electron microprobe results (in wt.%) of Cr-spinel and olivine from the Xiarihamu deposit.

Supplemental Table S5

Electron microprobe results (in wt.%) of Cr-spinel and olivine from the Shitoukengde mafic-ultramafic rocks

Supplemental Table S6

Whole-rock S concentrations (in wt.%) of the country rocks of the Xiarihamu Ni-Cu deposit and Shitoukengde mafic–ultramafic intrusion.

Supplemental Table S7

Representive whole-rock trace elements, Sr-Nd isotopes, orthopyroxene Mg isotope, and sulfide S isotope of the Xiarihamu Ni-Cu deposit and Shitoukengde mafic–ultramafic intrusion, and fO_2 values estimated using the Ol-Opx-Spl and Ol-Sul oxybarometers of several magmatic Ni-Cu deposits in China.

Fig.1

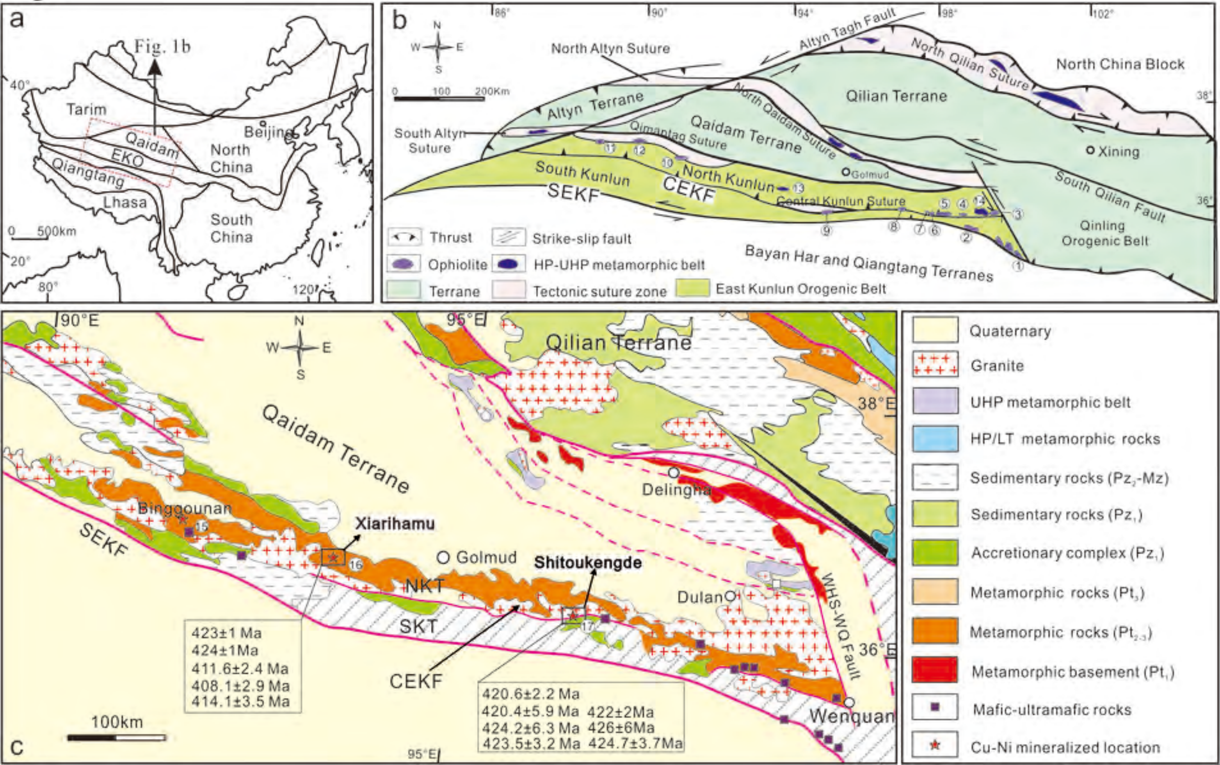

a
Fig. 1b
Tarim
Beijing
Qaidam
EKO
North China
Qiangtang
Lhasa
South China
0 500km
40°
20°
80°
120°
b
North Altyn Suture
Altyn Tagh Fault
North Qilian Suture
North China Block
Qilian Terrane
Altyn Terrane
North Qaidam Suture
South Altyn Suture
Qimantag Suture
Qaidam Terrane
Xining
Golmud
South Kunlun
North Kunlun
SEKF
CEKF
Central Kunlun Suture
South Qilian Fault
Qinling Orogenic Belt
Bayan Har and Qiangtang Terranes
0 100 200Km
Thrust
Strike-slip fault
Ophiolite
HP-UHP metamorphic belt
Terrane
Tectonic suture zone
East Kunlun Orogenic Belt
c
90°E
95°E
38°E
36°E
Qilian Terrane
Qaidam Terrane
Delingha
Binggounan
Xiarihamu
Golmud
Shitoukengde
Dulan
Wenquan
WHS-WQ Fault
SEKF
NKT
SKT
CEKF
100km
423±1 Ma
424±1Ma
411.6±2.4 Ma
408.1±2.9 Ma
414.1±3.5 Ma
420.6±2.2 Ma
420.4±5.9 Ma 422±2Ma
424.2±6.3 Ma 426±6Ma
423.5±3.2 Ma 424.7±3.7Ma
Quaternary
Granite
UHP metamorphic belt
HP/LT metamorphic rocks
Sedimentary rocks (Pz2-Mz)
Sedimentary rocks (Pz1)
Accretionary complex (Pz1)
Metamorphic rocks (Pt3)
Metamorphic rocks (Pt2-3)
Metamorphic basement (Pt1)
Mafic-ultramafic rocks
Cu-Ni mineralized location

Fig.2

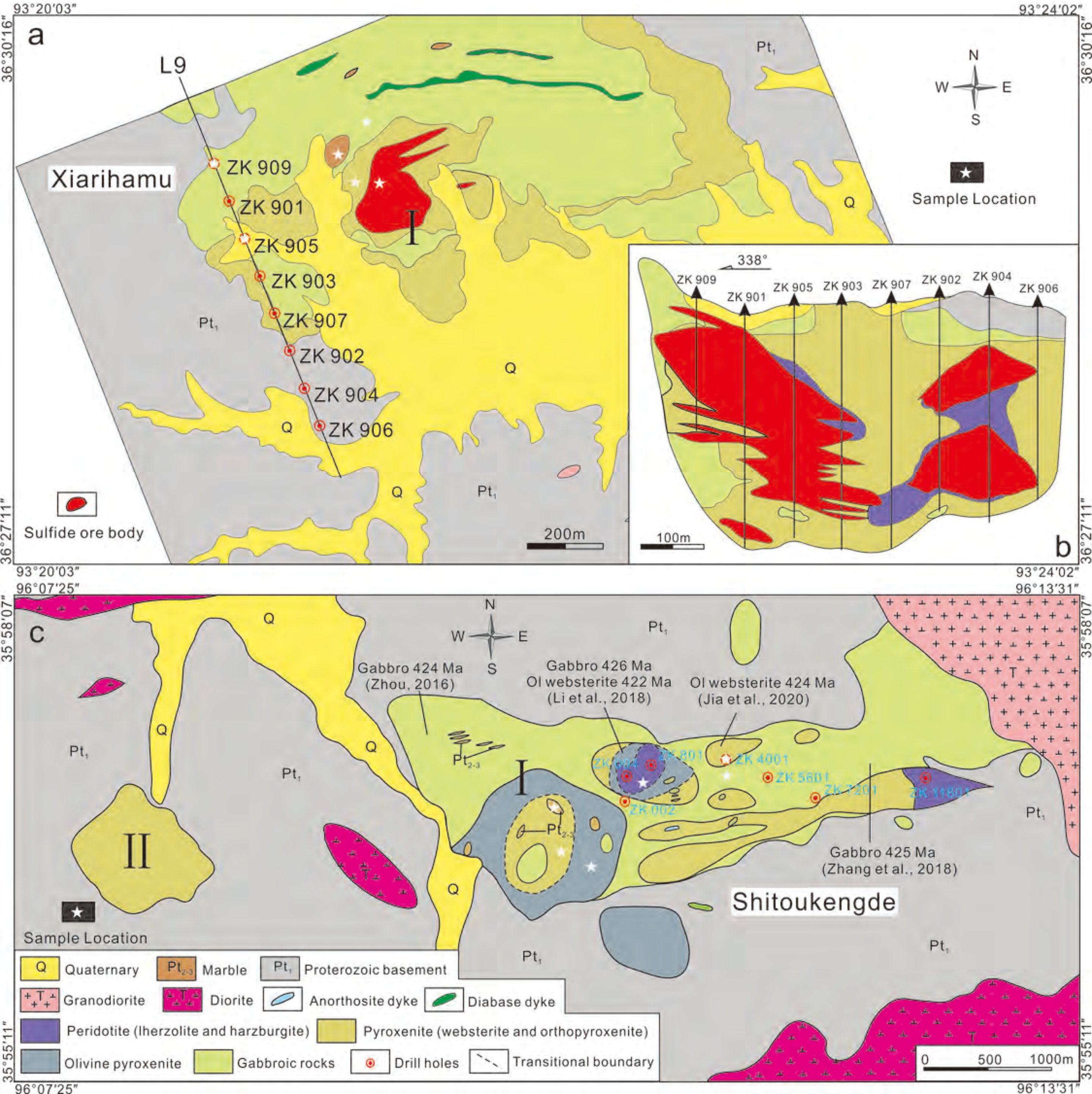

93°20'03"
93°24'02"
36°30'16"
36°27'11"
a
L9
Xiarihamu
ZK 909
ZK 901
ZK 905
ZK 903
ZK 907
ZK 902
ZK 904
ZK 906
I
Pt1
Q
N
W
E
S
Sample Location
Sulfide ore body
200m
b
338°
ZK 909
ZK 901
ZK 905
ZK 903
ZK 907
ZK 902
ZK 904
ZK 906
100m
96°07'25"
96°13'31"
35°58'07"
35°55'11"
c
Q
Pt1
Pt2-3
I
II
Gabbro 424 Ma
(Zhou, 2016)
Gabbro 426 Ma
Ol websterite 422 Ma
(Li et al., 2018)
Ol websterite 424 Ma
(Jia et al., 2020)
ZK 004
ZK 801
ZK 4001
ZK 5601
ZK 7201
ZK 11601
ZK 002
Gabbro 425 Ma
(Zhang et al., 2018)
Shitoukengde
T
Sample Location
Quaternary
Marble
Proterozoic basement
Granodiorite
Diorite
Anorthosite dyke
Diabase dyke
Peridotite (lherzolite and harzburgite)
Pyroxenite (websterite and orthopyroxenite)
Olivine pyroxenite
Gabbroic rocks
Drill holes
Transitional boundary
0
500
1000m

Fig.3

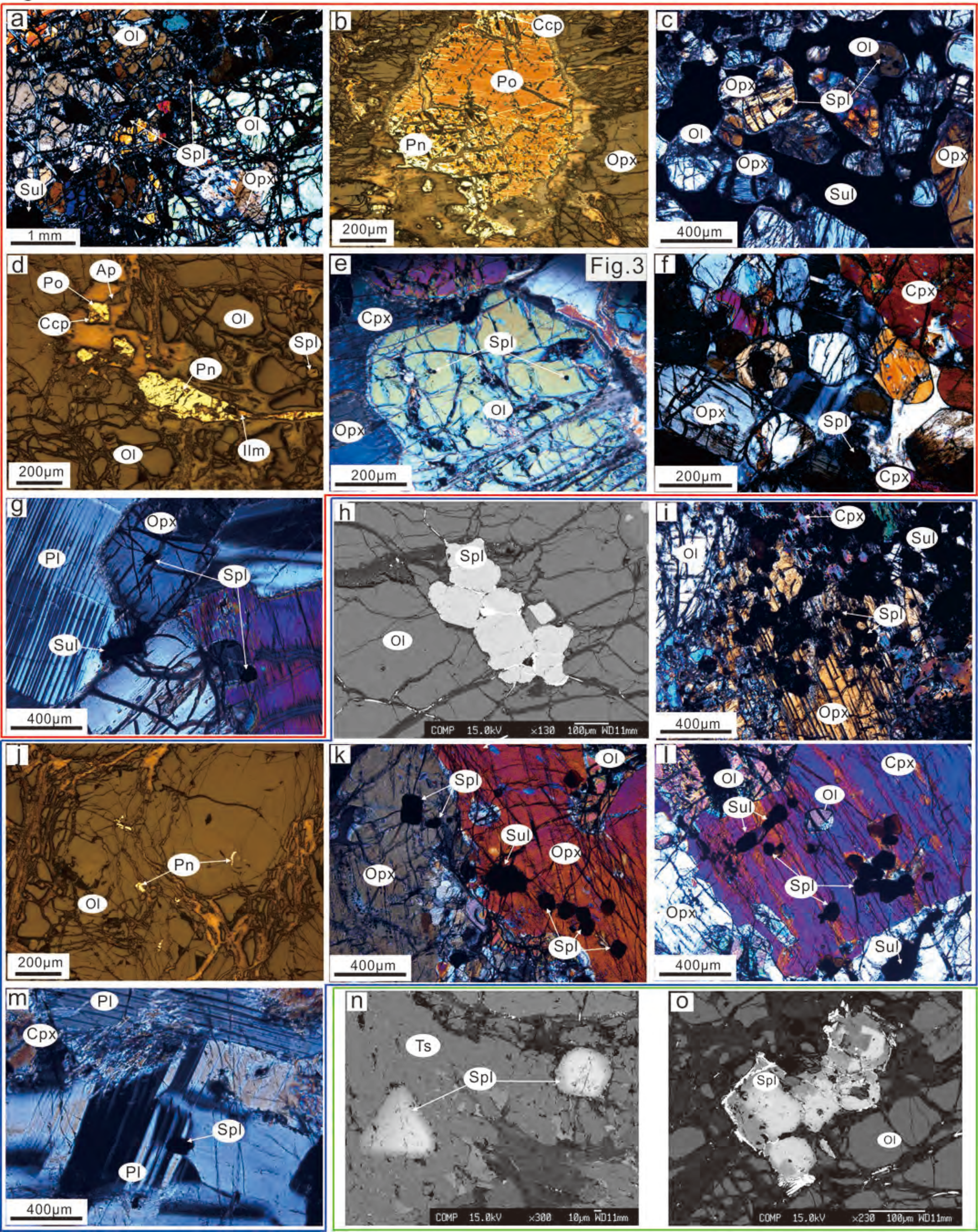
a
Ol
Ol
Spl
Opx
Sul
1 mm
b
Ccp
Po
Pn
Opx
200μm
c
Ol
Opx
Spl
Ol
Opx
Opx
Sul
400μm
d
Ap
Po
Ccp
Ol
Spl
Pn
Ilm
Ol
200μm
e
Fig.3
Cpx
Spl
Ol
Opx
200μm
f
Cpx
Opx
Spl
Cpx
200μm
g
Opx
Pl
Spl
Sul
400μm
h
Spl
Ol
COMP 15.0kV ×130 100μm WD11mm
i
Cpx
Ol
Sul
Spl
Opx
400μm
j
Pn
Ol
200μm
k
Ol
Spl
Sul
Opx
Opx
Spl
400μm
l
Cpx
Ol
Ol
Sul
Spl
Opx
Sul
400μm
m
Pl
Cpx
Spl
Pl
400μm
n
Ts
Spl
COMP 15.0kV ×300 10μm WD11mm
o
Spl
Ol
COMP 15.0kV ×230 100μm WD11mm

Fig.4

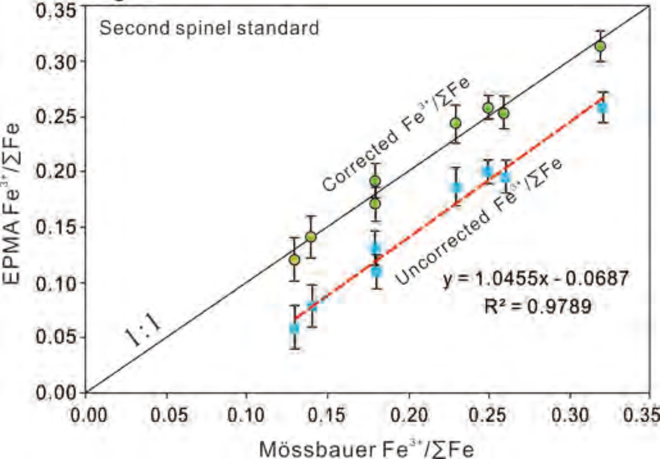

Second spinel standard
EPMA Fe3+/ΣFe
Mössbauer Fe3+/ΣFe
Corrected Fe3+/ΣFe
Uncorrected Fe3+/ΣFe
y = 1.0455x - 0.0687
R² = 0.9789
1:1
0.00
0.05
0.10
0.15
0.20
0.25
0.30
0.35

Fig.5

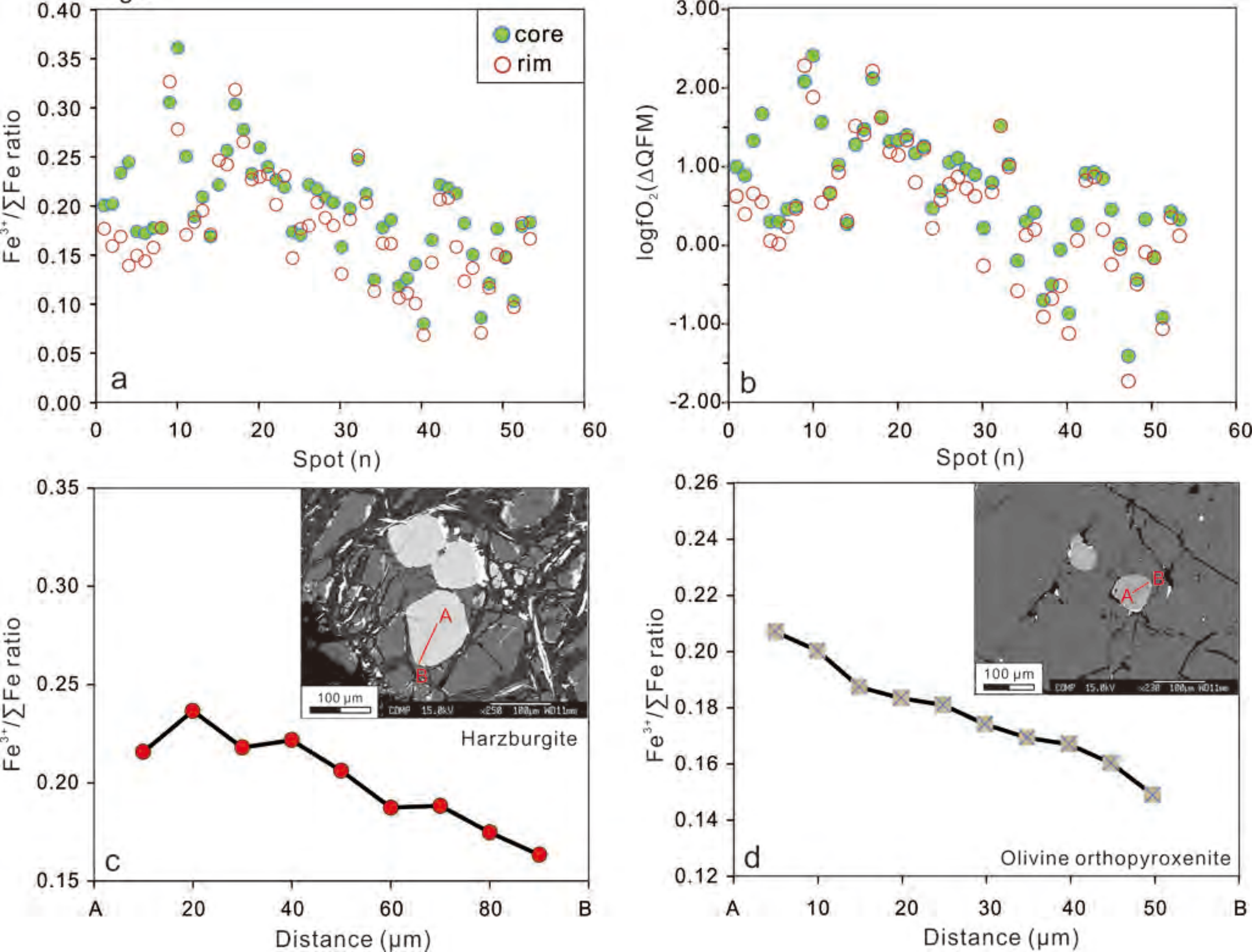
core
rim
a
b
c
d
Fe3+/∑Fe ratio
logfO2(ΔQFM)
Spot (n)
Distance (μm)
A
B
100 μm
COMP 15.0kV ×250 100μm WD11mm
COMP 15.0kV ×230 100μm WD11mm
Harzburgite
Olivine orthopyroxenite

Fig.6

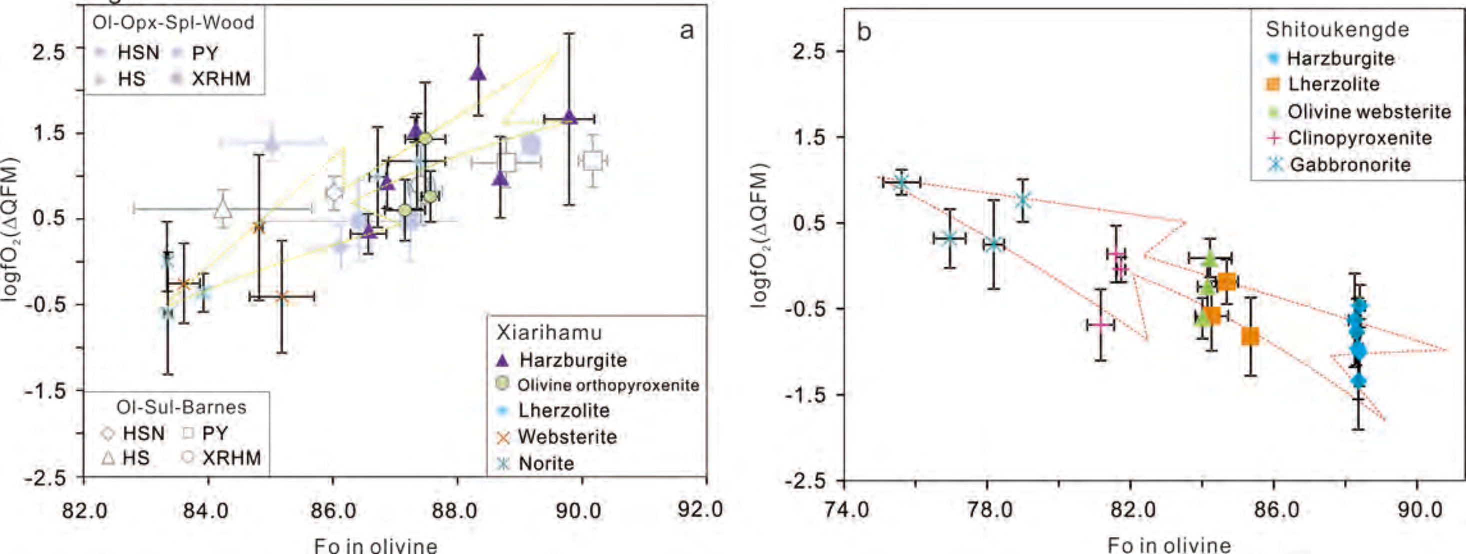

Ol-Opx-Spl-Wood
HSN
PY
HS
XRHM
a
2.5
1.5
0.5
-0.5
-1.5
-2.5
logfO2(ΔQFM)
Ol-Sul-Barnes
HSN
PY
HS
XRHM
Xiarihamu
Harzburgite
Olivine orthopyroxenite
Lherzolite
Websterite
Norite
82.0
84.0
86.0
88.0
90.0
92.0
Fo in olivine
b
Shitoukengde
Harzburgite
Lherzolite
Olivine websterite
Clinopyroxenite
Gabbronorite
74.0
78.0
82.0
86.0
90.0

Fig.7

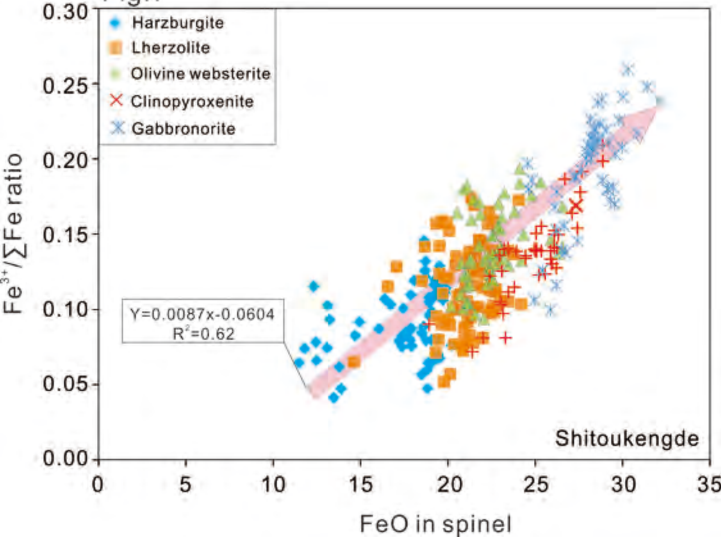

Harzburgite
Lherzolite
Olivine websterite
Clinopyroxenite
Gabbronorite
Y=0.0087x-0.0604
R^2=0.62
Shitoukengde
$Fe^{3+}/\sum Fe$ ratio
FeO in spinel
0.00
0.05
0.10
0.15
0.20
0.25
0.30
0
5
10
15
20
25
30
35

Fig.8

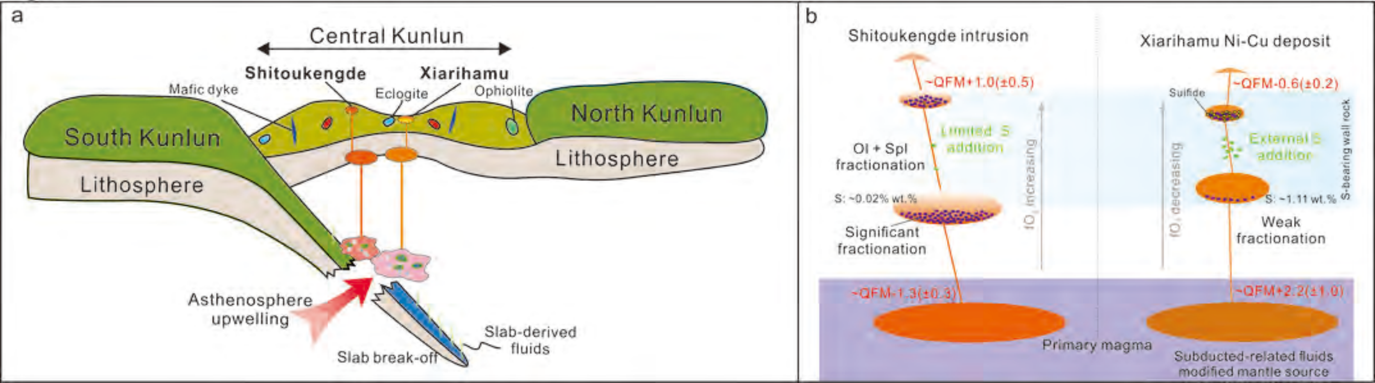

a
Central Kunlun
Shitoukengde
Xiarihamu
Mafic dyke
Eclogite
Ophiolite
North Kunlun
South Kunlun
Lithosphere
Lithosphere
Asthenosphere upwelling
Slab break-off
Slab-derived fluids
b
Shitoukengde intrusion
Xiarihamu Ni-Cu deposit
~QFM+1.0(±0.5)
Limited S addition
Ol + Spl fractionation
S: ~0.02% wt.%
Significant fractionation
~QFM-1.3(±0.3)
Sulfide
~QFM-0.6(±0.2)
External S addition
S-bearing wall rock
S: ~1.11 wt.%
Weak fractionation
~QFM+2.2(±1.0)
Primary magma
Subducted-related fluids modified mantle source